

Cranial anatomy of *Acynodon adriaticus* and extreme durophagous adaptations in Eusuchia (Reptilia: Crocodylomorpha)

Marco Muscioni^{1,2}  | Alfio Alessandro Chiarenza³  |
Diego Bladimir Haro Fernandez^{4,5}  | Diego Dreossi⁴  | Flavio Bacchia⁶ |
Federico Fanti^{1,2} 

¹Dipartimento di Scienze Biologiche, Geologiche e Ambientali, Alma Mater Studiorum, Università di Bologna, Bologna, Italy

²Museo Geologico Giovanni Capellini, Università di Bologna, Bologna, Italy

³Department of Earth Sciences, University College London, London, UK

⁴SYRMEP Group, Trieste, Italy

⁵Dipartimento di Fisica, Università della Calabria, Italy

⁶Zoic Limited Liability Company, Trieste, Italy

Correspondence

Marco Muscioni, Dipartimento di Scienze Biologiche, Geologiche e Ambientali, Alma Mater Studiorum, Università di Bologna, via Zamboni 33, 40126 Bologna, Italy.

Email: marco.muscioni2@unibo.it

Funding information

Zoic s.r.l.; NextGenerationEU - Piano Nazionale di Ripresa e Resilienza (PNRR) - XXXIX° cycle, STVA University of Bologna; Programma Operativo Nazionale (PON); Royal Society Newton International Fellowship, Grant/Award Number: NIF\R1\231802

Abstract

Acynodon adriaticus, a small eusuchian from the Late Cretaceous of Italy, is known for its well-preserved cranial and postcranial material. Despite its excellent preservation, many details remain hidden due to the physical overlap between the elements and matrix obliteration. We used Micro-CT scans to reveal previously overlooked anatomical features and describe in detail the cranial and dental anatomy of this taxon, shedding new light on its palaeoecology. The holotypic specimen, SC 57248, represents a mature individual exhibiting signs of hyperossification, developed ornamentation, and various pathologies, including jaw arthritis and a possible dental anomaly. *Acynodon adriaticus* exhibits significant durophagous adaptations, including a robust, brevirostrine skull optimized for powerful biting and stress-load capacity. Its specialized dentition, lacking caniniform teeth, features anterior chisel-like teeth and hypertrophic posterior molariforms with thick enamel, indicative of a diet specializing in hard-shelled prey. The dentition pattern, accelerated molariform replacement rate, and reduced orbit size suggest adaptations for durophagous foraging in turbid, densely vegetated aquatic environments. The paleoecological context during the Late Cretaceous, characterized by increased freshwater habitats and high invertebrate diversity, likely facilitated the evolution of such specialized traits in *A. adriaticus*. This small crocodylomorph likely foraged slowly in shallow, benthic environments, using its powerful bite to process mollusks and large arthropods. The study of *A. adriaticus*, along with comparisons with other crocodylomorphs and ecomorphologically similar taxa like *Iharkutosuchus makadii* and *Gnatusuchus pebasensis*, provides a valuable morphofunctional model for understanding the evolutionary pathways of extinct crocodylians to durophagy.

This is an open access article under the terms of the [Creative Commons Attribution](https://creativecommons.org/licenses/by/4.0/) License, which permits use, distribution and reproduction in any medium, provided the original work is properly cited.

© 2024 The Author(s). *The Anatomical Record* published by Wiley Periodicals LLC on behalf of American Association for Anatomy.

KEYWORDS

acynodon, cretaceous, durophagy, hylaeochampsidae, paleobiology

1 | INTRODUCTION

The Villaggio del Pescatore (VdP) site was discovered in November of 1984 by Giorgio Rimoli and Alceo Tarlao in the Cretaceous–Paleocene Karst beds exposed near Duino-Aurisina (northwest of Trieste, Italy) following reports of in situ vertebrate bones. Since then, dozens of limestone slabs have been quarried from the site, revealing a rich paleobiota that includes well-preserved vertebrates, invertebrates, and plants (Chiarenza et al., 2021; Consorti et al., 2021; Dalla Vecchia, 2009; Muscioni et al., 2024). Among tetrapods, the remains of a small crocodylomorph with well-preserved cranial material

(Figure 1a–d) were recovered and assigned to the genus *Acynodon* (*A. adriaticus*, Delfino et al., 2008), a southern European, Late Cretaceous endemic genus including two other known species (*A. iberoccitanus* and *A. lopezi*) and numerous fragmentary materials (see Buscalioni et al., 1997; Martin, 2007; Muscioni et al., 2023; Puértolas-Pascual et al., 2016).

Acynodon was previously considered an early diverging globidontan alligatoroid in accordance with other closely related European taxa. However, recent revisions of crocodylomorph phylogeny revealed that the genus, alongside other putative latest Cretaceous European alligatoroids, belongs to an unusual early diverging clade:

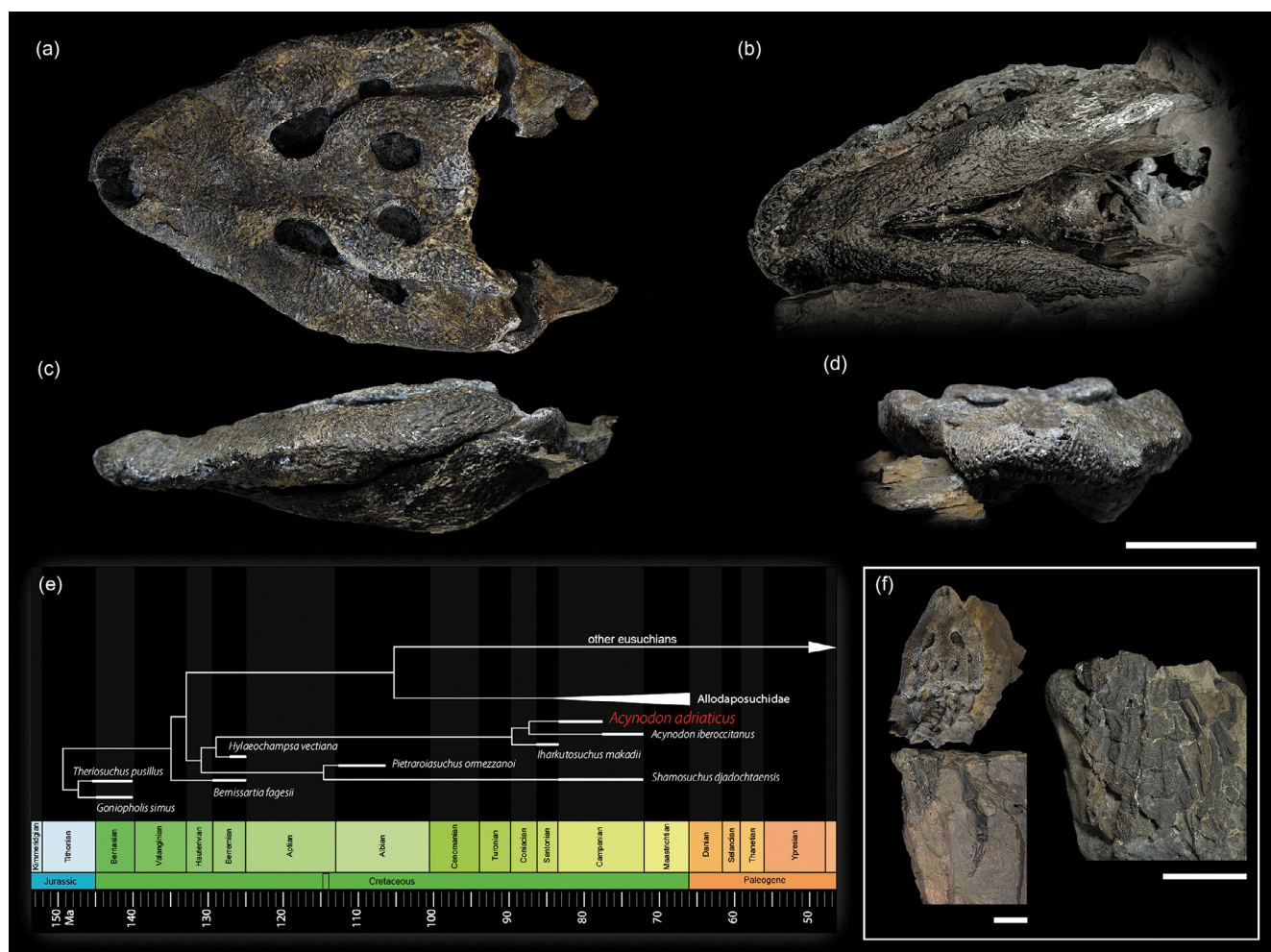


FIGURE 1 The skull of MCSNT 57248 in dorsal (a), ventral (b), lateral (c) and frontal (d) view. (e) simplified time-calibrated Bayesian tree of Hylaeochampsidae and close taxa at the base of Eusuchia, modified from Muscioni et al. (2023). (f) all fossil material representing or associated with the *Acynodon adriaticus* holotypic specimen; articulated blocks with the skull, cervical vertebrae and forelimb of MCSNT 57248 (left), and paravertebral osteoderm series and ribs of the paratype MCSNT 57032 (right). Scale bars = 50 mm.

Hylaeochampsidae (Brochu et al., 2012; Jouve et al., 2017; Martin et al., 2016; Muscioni et al., 2023; Narváez et al., 2015; Puértolas-Pascual et al., 2013). Anatomical differences observed between *A. adriaticus* and the other well-preserved congeneric species *A. iberoccitanus* suggest that the two taxa might not belong to a least inclusive monophyletic group and may belong to different genera (Muscioni et al., 2023; Ósi, 2014; Turner & Brochu, 2010). This conclusion is supported by most parsimony-based analyses, whereas the Bayesian analysis in Muscioni et al. (2023) recovered *Acynodon* as monophyletic, confirming the ambiguous status of this genus (Figure 1e). In addition, *A. adriaticus* shares with many other extinct eusuchians enlarged posterior teeth, suggesting some kind of dietary specialization.

This study focuses on the results of a series of micro-CT scans of the skull of the *Acynodon adriaticus* holotype (MCSNT 57248). Due to taphonomic distortion obscuring the ventral side of the skull and the dorsal view of the mandible, this is the first detailed and comprehensive description of the complete cranial anatomy of *Acynodon adriaticus*. The new morphological observations from the CT scans allowed for the separate analysis of the skull and mandible, revealing clear bone surfaces that were previously inaccessible. Additionally, the complete dentition of the specimen (including its replacement teeth) was successfully isolated, illustrated, and described. This information, along with the recent, renewed definition available for the holotype (Muscioni et al., 2023), allowed for the reliable assignment of another unrecovered in situ sectioned skull to *Acynodon adriaticus*. Finally, we integrate this new information with quantitative comparisons to other tetrapods to generate novel inferences about the paleobiology of this enigmatic and aberrant crocodylomorph.

2 | MATERIALS AND METHODS

2.1 | Specimens

Every fossil recovered from the VdP site is deposited at the Museo Civico di Storia Naturale di Trieste (MCSNT). The specimen MCSNT 57248 was discovered in 1998–1999 and includes the articulated skull, cervical vertebrae, right portion of the pectoral girdle with the right forelimb, a few ribs, and dorsal vertebrae with articulated paravertebral osteoderm armor. MCSNT 57248 is preserved in three distinct slabs: one containing the skull and cervical vertebrae, one containing the right forelimb, and the final one with the dorsal elements (Figure 1f). The first two blocks are inventoried together, whereas the

third block, which was found a few meters away, was given a different number (MCSNT 57032), sparking confusion about whether they represented associated material or different individuals. Both were described by Delfino et al. (2008) and designated respectively as holotype and paratype. No additional preparation was performed, and the current state of the specimen is the result of past chemical dissolution with formic acid and minor mechanical damage that occurred since 2008 (Figure S1). A non-inventoried, still in situ specimen is a partial left half of a skull with an articulated mandible, exposed as a slice on the quarry floor during quarrying activities in 1998–1999. Initially misidentified as a coprolite, a re-examination of the known in situ material in 2023 led to its definitive identification as a partial skull of *A. adriaticus* based on bone morphology and distinctive molariform teeth.

2.2 | Tomography

Cooperation between the University of Bologna Alma Mater Studiorum, the University of Trieste, Museo Civico di Storia Naturale di Trieste, ZOIC s.r.l., and Elettra-Sincrotrone Trieste under an Accordo Quadro agreement allowed the digitization and μ -CT scanning of the specimens. Physical preparation of the specimen for tomography was carried out by ZOIC s.r.l. by encasing the fossil in a stabilizing polyurethane foam shell, and then mounting it on a custom wooden base with an adjustable screw pin for the tomographer's base. Thirteen stacked acquisitions in total, of which nine are used herein, were carried out at the x-ray microtomography laboratory of Elettra (FAITH) with the following parameters. x-Ray source (Hamamatsu L12161-07) settings: HV = 145 kVp; I = 450 μ m, focal Spot = 50 μ m. Filters: 2 mm copper plus 2.25 mm brass. Detector: Dalsa Shad-O-Box 6 k HS, matrix 2940 \times 2304, pixel size 49.5 μ m, and active area of 145 \times 114 mm². Geometry: source distance = 380 mm, detector distance = 627 mm, equivalent pixel 30 μ m. Local Area CT acquisition: 3600 projections with exposure time of 4 s. Reconstruction software: NRecon v 1.6.9.18, Bruker. Data stitching was performed using the software PerGeos, while segmentation was done using Avizo 3D 2021.1. The physical properties of the large volumes of matrix still encasing the skull produced very undefined imagery, and very few internal anatomical structures were recognizable. However, thin to medium volumes of matrix, resins, and synthetic consolidants filling small superficial crevices and foramina were easily identified and digitally removed through meticulous slice-by-slice visual identification and first-hand processing. This CT scan is available on the online repository MorphoSource

with the Media ID 000641787 (alongside the derived 3D mesh models of the skull, upper and lower dentition) and is accessible at this link: <https://www.morphosource.org/concern/media/000641787?locale=en>.

2.3 | Imaging

Photographs of the specimens were taken with a SONY DSC-RX100M3 camera and a pocket USB microcamera. Meshes exported from Avizo were visualized and snapshot on Meshlab 2022.02.

2.4 | Quantitative analysis

We compiled an enamel dataset (Supplementary Information S2) by surveying the literature and accessing thin-sections and whole teeth samples at the Museo Geologico Giovanni Capellini (MGGC) of fossil and living tetrapods. Average skull length of available taxa was measured from the tip of the premaxillae to the posteroventral most corner of either the quadrate or the squamosal; when this measure was not available or accessible (~50% of considered specimens) it was approximated at reasonable values based on comparisons with closely related or more complete specimens. The widely used dorsal cranial length (DCL) was evaluated as potentially problematic as skull-length measure due to the diversity of the cranial morphologies and functionality in the sample, and thus not used as a reference measurement. The raw dataset with data sources is available in the Supplementary Information S2.

3 | RESULTS

3.1 | Systematic paleontology

Crocodylomorpha Hay, 1930 sensu Nesbitt, 2011.

Neosuchia Benton & Clark, 1988.

Eusuchia Huxley, 1875 sensu Brochu, 2003.

Hylaeochampsidae Andrews, 1913.

Acynodon Buscalioni et al., 1997.

Acynodon adriaticus Delfino et al., 2008.

3.2 | Comparative description

3.2.1 | General description of the skull

The skull measures 155 mm in length from the tip of the premaxillae to the posterior margin of the quadrates,

with a dorsal cranial length of 140 mm (see Table 1 for other linear measurements). It has a wide, triangular shape with an acute rostrum and expanded posterolateral region (Figures 1 and 2). The skull is dorsoventrally compressed and has undergone both ductile and brittle diagenetic deformation (see Supporting Information). The preorbital portion of the snout is collapsed along a U-shaped fracture parallel to the labial margin and reaching the naris (Figure 3a), while the skull roof is plastically flattened. The skull is visibly brevirostrine and stout. In its deformed state, the snout-skull length ratio is approximately 0.4, comparable to that of *A. iberoccitanus* (Martin, 2007; Figures 1 and 3). Similarly, the ratio between the mediolateral width of the rostrum at the level of the orbits and the width of the skull table is ~1.5.

TABLE 1 Linear measurements of the holotypic skull MCSNT 57248.

Linear measures	Values (mm)
Total cranial length ^a	155
Dorsal cranial length ^b	140
Snout length ^c	64
Maximum cranial width ^d	119
Braincase width ^e	74
Interorbital width ^f	21
Snout width ^g	96
Rostrum width ^h	40
External naris width	21
Individual width of quadrate condyle	23
Orbit length	23
Orbit width	15
Infratemporal fenestra length	16
Supratemporal fenestra length	17
Supratemporal fenestra width	14
Suborbital fenestra length	30
Total mandible length ⁱ	180
Retroarticular process length ^j	29
Symphysis length	30
Occipital condyle width	7.8

^aFrom anterior margin of premaxillae to posterior margin of quadrates.

^bFrom anterior margin of premaxillae to the posterior margin of supraoccipital.

^cFrom anterior margin of premaxillae to the anterior margin of orbits.

^dWidest point corresponding to the lateral margin of the jugals.

^eFrom left to right squamosal prong.

^fRoughly at the contact between frontal and prefrontals.

^gMeasured at the level of the anterior margin of orbits.

^hMeasured at the premaxillae-maxillae suture along the oral margin.

ⁱMeasured in lateral view.

^jMeasured along the retroarticular process' axis.

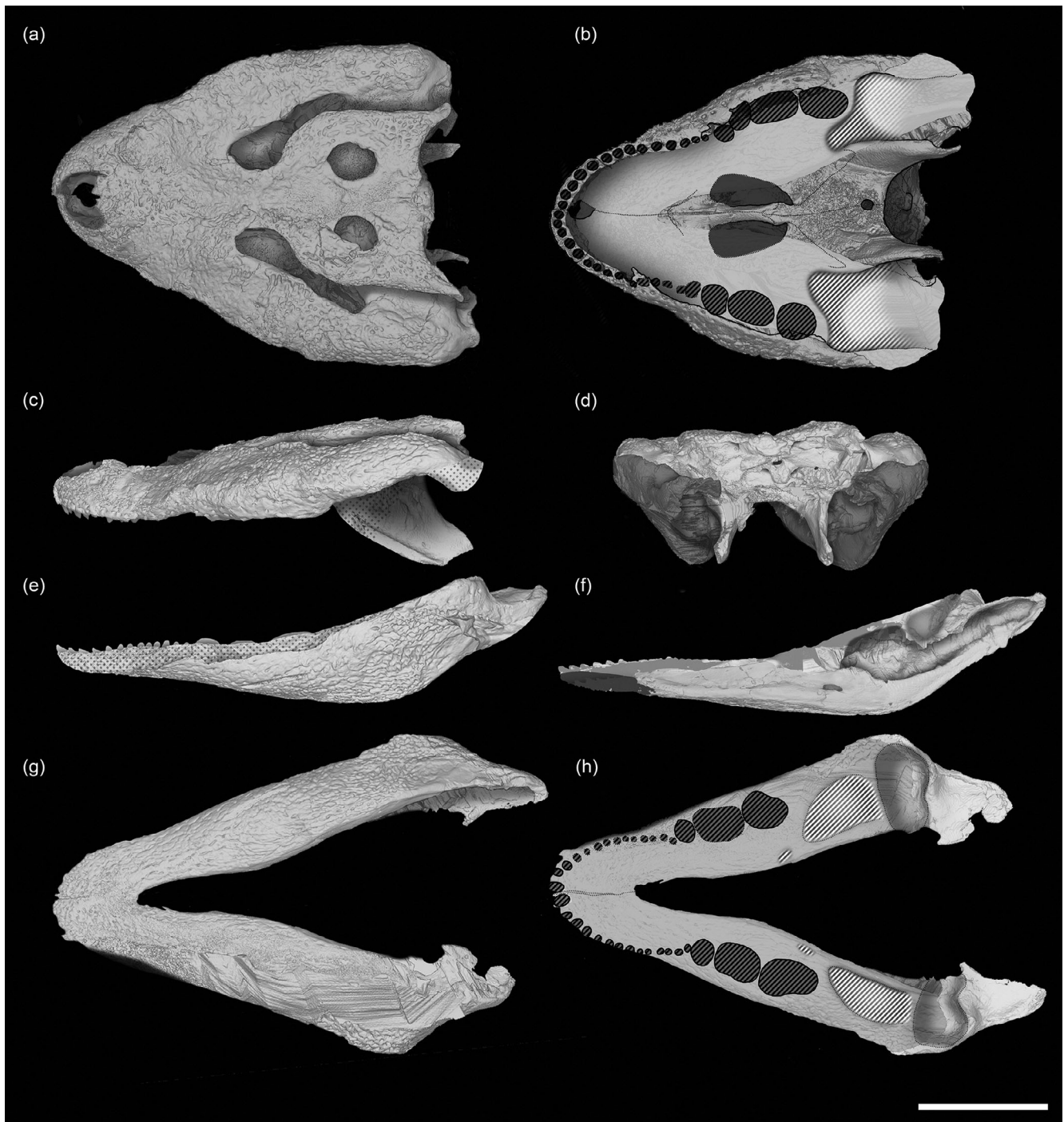


FIGURE 2 Surface renderings of the segmented MCSNT 57248 skull and mandible in various views. Skull: Dorsal (a), ventral (b), lateral (c), and posterior (d). Mandible: Posterior (darker) (d), lateral (e), medial (f), ventral (g) and dorsal (h). Dark barred areas represent the putative alveoli, and light barred areas represent cavities with interpretative uncertainties (b, h). Dotted areas in (c) and (e) represent inferred bone surfaces not isolated through segmentation. Dotted lines in (b) indicate rough sutures, and homogeneous gray in (f) indicates the symphyseal surface. Scale bar = 50 mm.

For comparison, these values are 0.43 and 1.6 in *A. iberoccitanus*, 0.5 and 1.7 in *Caiman latirostris*, 0.48 and 1.0 in *Paleosuchus palpebrosus*, and 0.56 and 1.17 in a personally inspected juvenile *Crocodylus niloticus* of comparable skull size.

As reported by Delfino et al. (2008), the sutures are extensively closed with fused margins, making the identification of individual bones difficult. Tomographic scans allow for a more precise assessment of cranial elements (Figure 4). The pits and ridges of the superficial

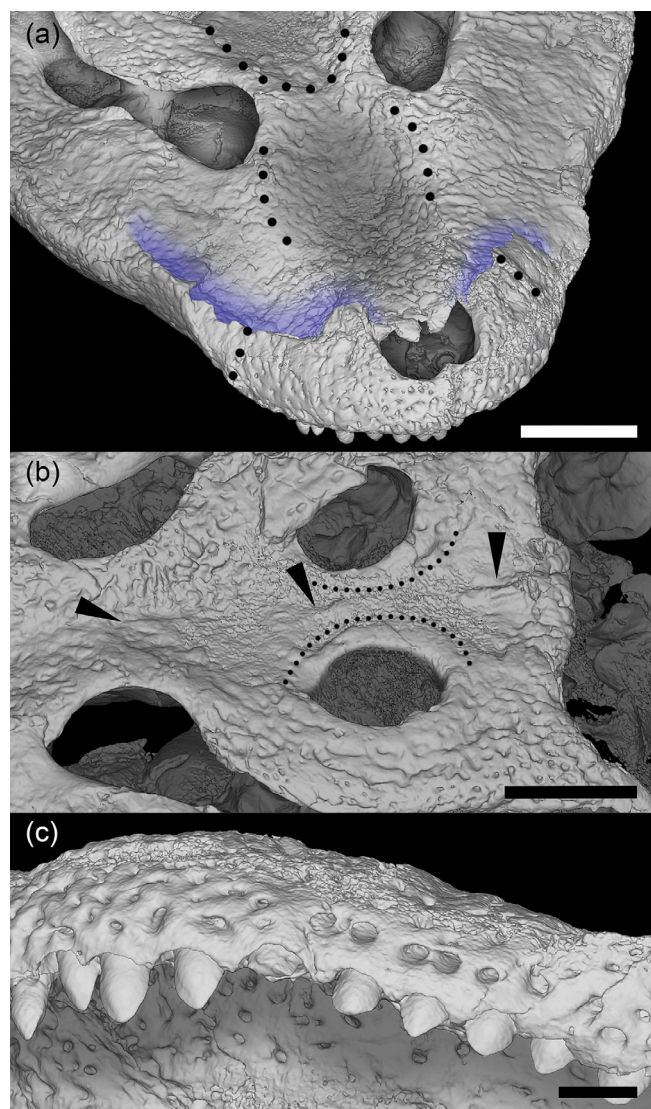


FIGURE 3 Details of dorsal and labial cranial features of MCSNT 57248. (a) orbital and preorbital portion of the skull in frontodorsal view. Dotted lines highlight the putative interorbital ridge and *canthi rostralii*-like dorsorostral ridges. The arched collapse fracture is highlighted in blue. (b) laterodorsal view of the skull table. Dotted lines highlight the thickened medial margins of the supratemporal fenestrae. Black arrows point to the sagittal keel reaching the interorbital area from the supraoccipital. (c) ventrolateral view of the right premaxillary-maxillary labial margins. Note the diameter of the labial foramina overlying the teeth alveoli. Scale bars = 20 mm (a, b), 5 mm (c).

ornamentation are well developed and deeply sculptured. In crocodylians the superficial texture of cranial dermal bones progressively becomes more deeply sculptured with age; this, alongside extensive cranial sutural fusion, cranial proportions, robustness, and cervical neurocentral suture fusion supports a mature ontogenetic stage of the specimen at the time of death (Griffin et al., 2021; Grigg & Kirshner, 2015). Although a true spectacle is absent as reported by Delfino et al. (2008), a slightly thickened bar

between the orbits may indicate a poorly prominent interorbital ridge (Figure 3a), less developed than in *A. iberoccitanus* and more similar to that of *Alligator mississippiensis*.

Despite the compression and fragmentation of the rostrum, two poorly developed ridges reminiscent of *canthi rostralii* (sensu Rio & Mannion, 2021) can be observed as low, gently arched ridges extending from the anterior area of the orbits, seemingly converging toward the external naris (Figure 3a,b), although there may be a hint of lateral orientation at the premaxillae-maxillae suture. The shape of the ridges is almost identical to those in *A. iberoccitanus* (see Martin, 2007, Figures 1 and 2) and their height from the rostrum level is similar to that in *Caiman latirostris*. The rest of the rostrum has a homogeneous rugose texture on its dorsal surface.

The largest and deepest ornamentations are on the dorsolateral surface of the lacrimal, jugal, and quadratojugal, forming elongated grooves with an anteroposterior orientation on the left jugal and a radial orientation along the left orbit. On the cranial roof, the ornamentation is most developed on the dorsolateral surface of the squamosal and postorbital. Two slightly depressed, mediolaterally symmetric areas are present on the skull table: one on the frontal between the orbits and supratemporal fenestrae (also observed in *A. iberoccitanus*), and the other on the parietal behind the supratemporal fenestrae (Figure 3b).

Certain traits of the skull ornamentation are considered diagnostic for *A. adriaticus* (Delfino et al., 2008). In *A. iberoccitanus*, a sagittal keel is present along the frontal and parietal, with maximum development between the orbits. In *A. adriaticus*, this structure is more developed between and posterior to the supratemporal fenestrae, bisecting the posterior depressed surface on the parietal (Figure 3b). The thickened medial margins of the supratemporal fenestrae and the smooth posterodorsal surface of the squamosals were also considered diagnostic. However, the thickened medial margin of the supratemporal fenestrae is ambiguous, as *A. iberoccitanus* skulls show similar thickening, although with different proportions (see Martin, 2007). The dentigerous margin of the premaxillae, maxillae, and dentary are regular and continuous, not interrupted by any notches or significant curves. Toward the labial margins foramina become progressively larger and more numerous, leading to a row of very large labial foramina running parallel to the upper teeth row just dorsal to the alveoli. Some of these foramina are nearly as large as the smaller maxillary alveoli (Figure 3c).

3.2.2 | Premaxillae and maxillae

The premaxillae are unfused and more mediolaterally than anteroposteriorly developed, with two elongated

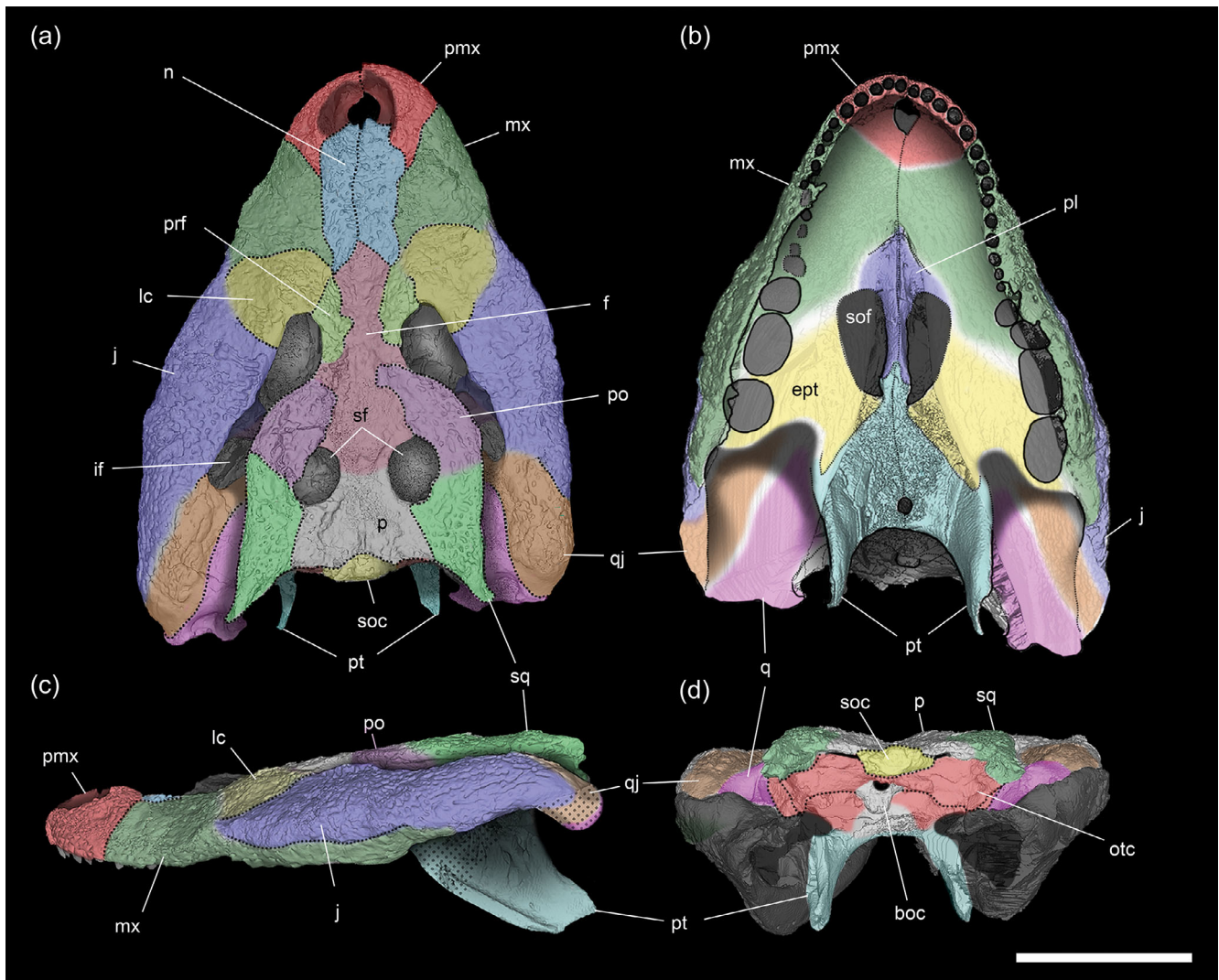


FIGURE 4 Schematic individual cranial bones of MCSNT 57248 in dorsal (a), ventral (b), lateral (c) and posterior (d) view. Individual elements are highlighted in coherent colors. Dotted lines represent putative sutural margins, and shaded white areas represent inferred sutural margins not possible to identify with certainty. Dotted areas in (c) represent inferred bone surfaces not isolated through segmentation. Scale bar = 50 mm. boc, basioccipital; ept, ectopterygoid; f, frontal; if, infratemporal fenestra; j, jugal; lc, lacrimal; mx, maxilla; n, nasal; otc, otoccipital; p, parietal; pl, palatine; pmx, premaxilla; po, postorbital; prf, prefrontal; pt, pterygoid; q, quadrate; qj, quadratojugal; sf, supratemporal fenestrae; soc, supraoccipital; sof, suborbital fenestra; sq, squamosal.

caudal processes contacting the lateral margins of the nasals (Figure 4). They almost exclusively surround the external naris, with only the posterior margin bordered by the nasals. The external naris is relatively small, bilobate, and subcircular with a length-width ratio of ~ 1 ; for comparison, this ratio is ~ 1.3 in *A. iberoccitanus* ACAP-FX1, 1.7 in juvenile *Crocodylus niloticus*, and 0.9 in *Osteolaemus tetraspis* (sensu Rio & Mannion, 2021; Appendix 2, character 3). It is dorsally and slightly anteriorly oriented, hinting at an original anterodorsal orientation (Figure 5a). The external naris is positioned very close to the tip of the snout, showing a slight anterior emargination. The ratio between the anterior premaxillary margin thickness and naris length

(sensu Rio & Mannion, 2021; Appendix 2, character 4) is about 0.2. The incisive foramen is visible from the naris and has an elliptical outline, slightly narrower than it is long (Figure 5b). It is relatively small, with the ratio between its maximum width and the snout width at the premaxillary-maxillary suture (sensu Rio & Mannion, 2021; Appendix 2, character 12) being ~ 0.2 .

Each premaxilla bears three main neurovascular foramina on the anterior vertical wall of the narial fenestra (with the left one having four; Figure 5c). They communicate directly with the labial foramina through the premaxillary neurovascular network vacuity, a condition also seen in some inspected *A. mississippiensis* specimens (Figure 5e). These can be at least partially identified as

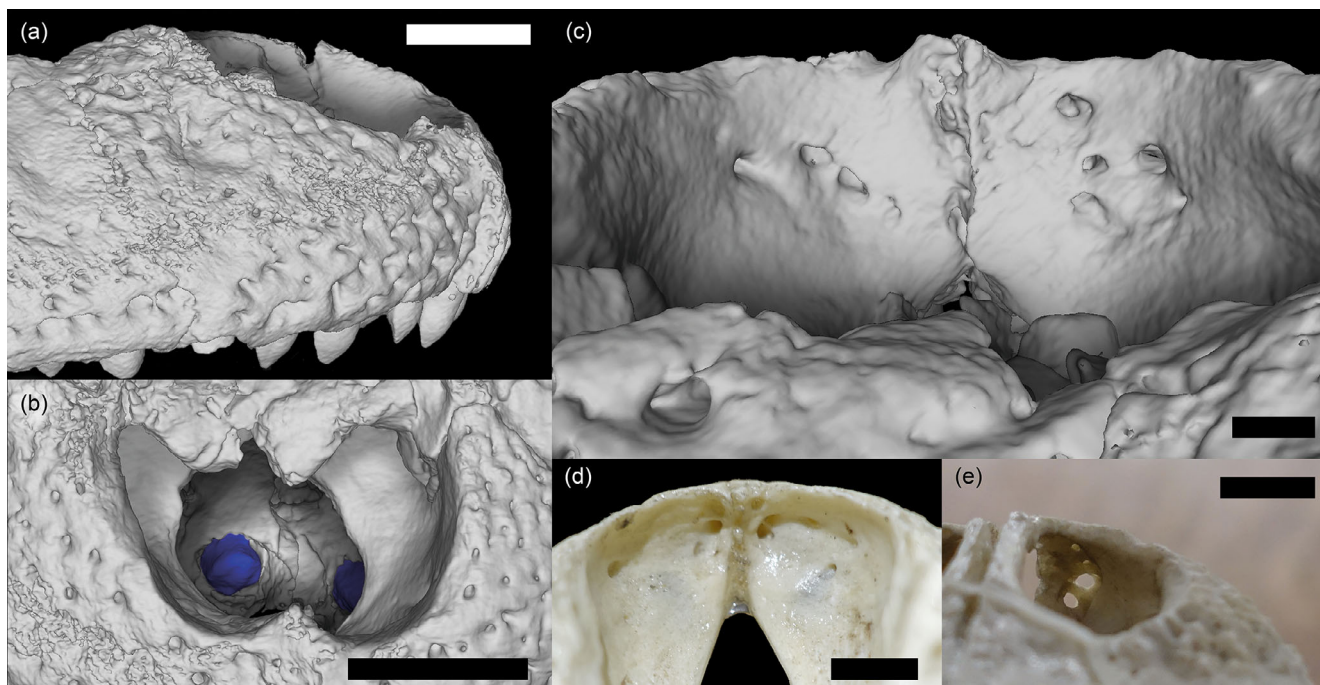


FIGURE 5 Detail of the narial region of MCSNT 57248. (a) premaxillae and naris in lateral view. Note the anterodorsal orientation of the naris and abundant premaxillary foramina. (b) dorsofrontal view of the naris, highlighting the incisive foramen and distal symphyseal portion of the mandible with two dentary teeth (blue). (c) large neurovascular foramina on the anterior naris wall, and the same structures in *Caiman* sp. (d) and *Alligator mississippiensis* (e). Scale bars = 10 mm (a, b, d, e), 1 mm (c).

passages of the narial circulation highlighted by Porter et al. (2016). Each premaxilla bears 5 alveoli. The premaxillary secondary palate is largely obscured by the occluding mandible; the latter is however slightly posteriorly displaced, leaving around 5 mm of visible surface just behind the anterior alveoli. This surface bears many small foramina on the lingual bony wall arranged in a parallel line to the dentigerous margin. In addition, small occlusal pits can be observed between some alveoli, specifically between P1 and P2, P3–P4, P4–P5.

The brevirostrine proportions of the skull result in the maxilla not being particularly developed dorsally but having a long lateroventral posterior ramus reaching the level of the infratemporal fenestra. Its contact with the nasal and lacrimal is mostly unrecognizable, inferable only by the orientation and consistency of shallow sulci and cracks which are easily confused with the ornamentation (Figure 4a). The posterior end is well defined, forming a narrow arch under the jugal around the last, massive molariform-shaped alveolus (Figure 4c). The posterior extremity of the maxilla extends past the postorbital bar to the level of the infratemporal fenestra, with a triangular posterior process reminiscent of *Iharkutosuchus makadui*. The palatal portion of the maxilla is not visible but given the skull proportions and the anterior level of the suborbital fenestrae, it must have been less anteroposteriorly expanded than in *A. iberoccitanus* and

I. makadui. Hints of bone septa from the crushed small caviconchal fossae can be observed in CT slices (Figure S3). The maxilla bears 13 alveoli.

3.2.3 | Palatine

The palatines are exposed in ventral view with well-preserved sutures (Figure 6), though skull deformation has resulted in a position almost attached to the ventral surface of the frontal. Maxillary processes extend to the level of the fifth maxillary alveolus, converging medially to form a rostral acute shape followed by posterolaterally oblique margins. One relatively large anterior palatine foramen is asymmetrically preserved in both the left and right elements, with the right side being more caudally positioned. Smaller foramina are preserved more caudally, in front of the suborbital fenestrae. The suborbital fenestrae, which are anteromedially completely formed by the palatines, have an elongated oval shape with medially arching posterior edges. The suborbital fenestrae are proportionally longer than in other well-known hylaeochampsids (17% of the skull length in *A. iberoccitanus* ACAP-FX1, 16% in *I. makadui* MTM 2006.52.1, and 20% in *A. adriaticus* MCSNT 57248) but slightly less so than in modern brevirostrine eusuchians (25.7% in *Caiman latirostris* and 39% in *Osteolaemus tetraspis*).

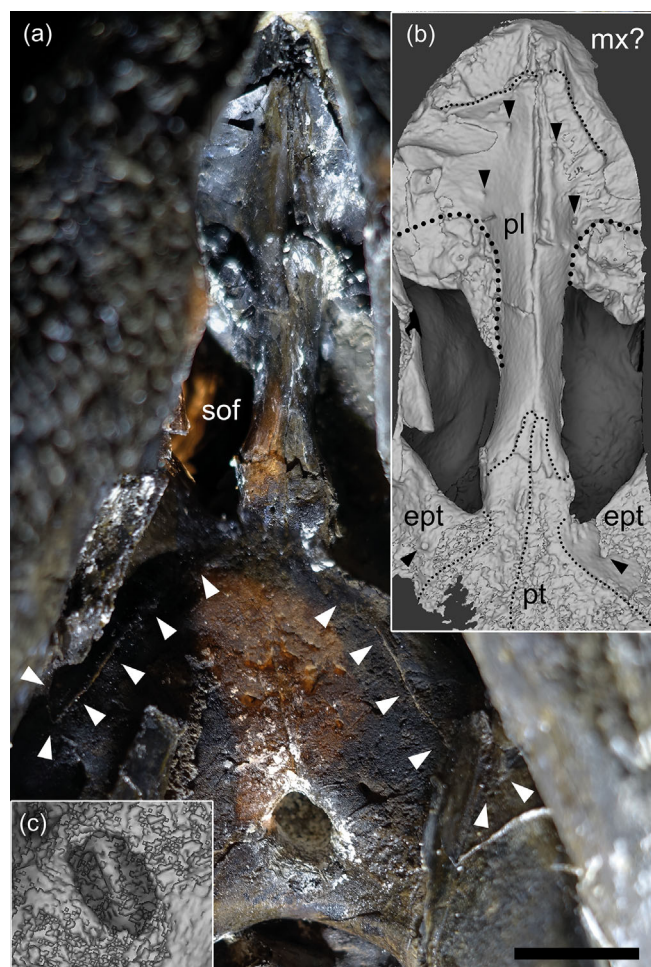


FIGURE 6 Detail of the visible palatal region of MCSNT 57248 (a) and surface rendering of the same area (b). Smaller dotted lines represent putative bone sutures, larger dotted lines represent the anterior margins of the suborbital fenestrae. Black arrows highlight the large palatine and ectopterygoid foramina, white arrows highlight the visible contact between ectopterygoids and pterygoids. Panel (c) represents the septate choana as visible in the tomographic data. Note the contrast between the photo and the surface rendering of the pterygoid bone around the choana: Relatively smooth in direct observation, irregular and porous under CT, indicating low density or acid dissolution damage. Scale bar = 10 mm. ept, ectopterygoid; mx, maxilla; pl, palatine; pt, pterygoid; sof, suborbital fenestra.

They are relatively mediolaterally narrow compared to *A. iberoccitanus* and living brevirostrine taxa, but proportionally similar to those of *I. makadaii* and *Hylaeochampsa vectiana* (the ratio between maximum width and maximum length of the fenestrae is 0.4 in *A. iberoccitanus*, 0.3 in *I. makadaii*, ~0.28 in *H. vectiana*, 0.38 in *A. adriaticus*, 0.55 in *C. latirostris*, and 0.4 in *O. tetraspis*). They are placed relatively anteriorly, with the rostral margin almost reaching the level of the 13th alveolus (M8), while in *I. iberoccitanus* and *I. makadaii* it reaches the 16th tooth

position (M10–M11). The pterygoid processes are very thin and form most of the palatal bar. Compressive forces likely caused the “median groove” of the palatal bar mentioned by Delfino et al. (2008), where the two halves disarticulated along the medial suture and slightly laterally rotated along their axis. The palatine bar is narrower than in other hylaeochampsids but proportionally similar at its minimum value to modern taxa: the ratio between the minimum width of the palatine bar and the width of the fenestrae at the same level is 0.40 in *A. iberoccitanus*, 0.50 in *I. makadaii*, 0.20 in *A. adriaticus*, 0.20 in *C. latirostris*, and 0.24 in *O. tetraspis*. The same ratio is closer to 0.40 in *Hylaeochampsa*, but is more difficult to compare as its palatine bar has a very homogeneous width. The contact with the pterygoids is near the posterior end of the suborbital fenestrae, corresponding to a slight enlargement of the palatal bar. The suture on each side has a developed caudolateral process creating a forked morphology, with the medial space filled with two thin palatine processes of the pterygoids in a wedge-shaped, slightly asymmetrical structure.

3.2.4 | Ectopterygoid and pterygoid

The ectopterygoids are partially visible, bordering the caudolateral margins of the suborbital fenestrae and the anterior portion of the pterygoid processes (Figure 6). Two large foramina are located just behind the suborbital fenestrae. Their contact with the pterygoids is represented by two faint symmetrical sutures directed caudolaterally, with the most caudal portion of the bone placed anterior to the level of the choana, as in *Hylaeochampsa* and *Iharkutosuchus*. CT data and comparison with *I. makadaii* suggest that the maxillary processes had significant lateral development, forming the medial portion of the large maxillary molariform alveoli. Their involvement in the pterygoid flanges is minimal. The pterygoids have slightly elongated palatine processes, forming the posteromedial margin of the suborbital fenestra. Several foramina are preserved on the ventral pterygoid surface anterior to the choana. The pterygoid surface around the choana is smooth and relatively flat, forming a roughly quadrangular surface enclosed between the ventromedial surfaces of the pterygoid flanges. Tomographic data reveal that the bone in this area has significantly lower density than the surrounding bone, making it difficult to distinguish from the matrix or rendering it invisible (hence the “noisy” surface in Figure 6c). The choana is oval-shaped and positioned just behind the level of the last maxillary alveolus. It lacks a bony neck, edges, or visible septum; however, CT data reveal a laterally crushed recessed septum starting just below the currently

obstructed passage (Figures 6c and S6). The pterygoid flanges are similar to those of *I. makadii* and differ significantly from those in living eusuchians. They are vertical, caudally arched, “boomerang-shaped” processes with minimal mediolateral expansion, extending slightly more posteriorly than the quadrate condyles (Figure 7). At least two foramina are visible on the lateroventral surface of the left pterygoid flange. The distal portion of the flanges has surface striations, less visible on the incomplete right flange (Figure 7b,c). The pterygoid buttress is proportionally similar to those in other taxa.

3.2.5 | Nasal

The exact shape of the nasals is difficult to determine due to damage and deformation of the dorsal surface of the rostrum. They form part of the posterior margins of the external naris and only slightly bisect the opening with two separate anterior ends, reaching less than half the rostrocaudal length of the naris. Just before entering the naris, the two extremities appear mediolaterally enlarged, with the two small anterior processes not representing a continuation of the converging lateral margins. These seem slightly posteriorly diverging, leading to two pointy posterior processes separated by the frontal.

3.2.6 | Lacrimal, prefrontal, and frontal

The contacts between the maxillae, lacrimals, and prefrontals are completely obscured by ornamentation and

sutural fusion (Figures 2a and 4a). The lacrimal and prefrontal appear as a single bony shield, making any remarks about their proportions speculative. On the anterior edge of the orbits, where the lacrimal and prefrontal would supposedly meet, small, slightly raised rugosities correspond to the beginning of the low *canthi rostralii* (Figure 3a,b). The right prefrontal can be identified as a hatchet-shaped element on the anteromedial margin of the orbit, while the left lacrimal can be identified as a larger, subcircular bone with a rounded lateral outline on the anterolateral margin of the orbit. Following this interpretation, the posterior processes of the nasals would either contact or be very close to both the anterior end of the prefrontals and the medial process of the lacrimals. The left and right prefrontals are separated by the frontal.

The crushed prefrontal pillars are still preserved, visible through the anterior medial margins of the orbits (Figures 8a and S3). The orbits are elongated and small relative to the skull size, with an anteroposterior length of ~23 mm from the anterior tip to the rostradorsolateral most point on the rostral face of the postorbital bone (sensu Cerio & Witmer, 2022). The ratio between the rostrocaudal orbit length and skull length in dorsal view is 0.14, more in line with larger and non-brevirostrine taxa (0.18 in juvenile *C. niloticus*) than in the related *A. iberoccitanus* (~0.22) or the similarly sized and brevirostrine *O. tetraspis* (~0.24). The shape of the right orbit is probably less deformed. Their dorsal orientation is likely close to the original position, as seen in *A. iberoccitanus* and many other extinct and extant eusuchians (e.g., *Caiman latirostris*; Muscioni, personal observation 2023).

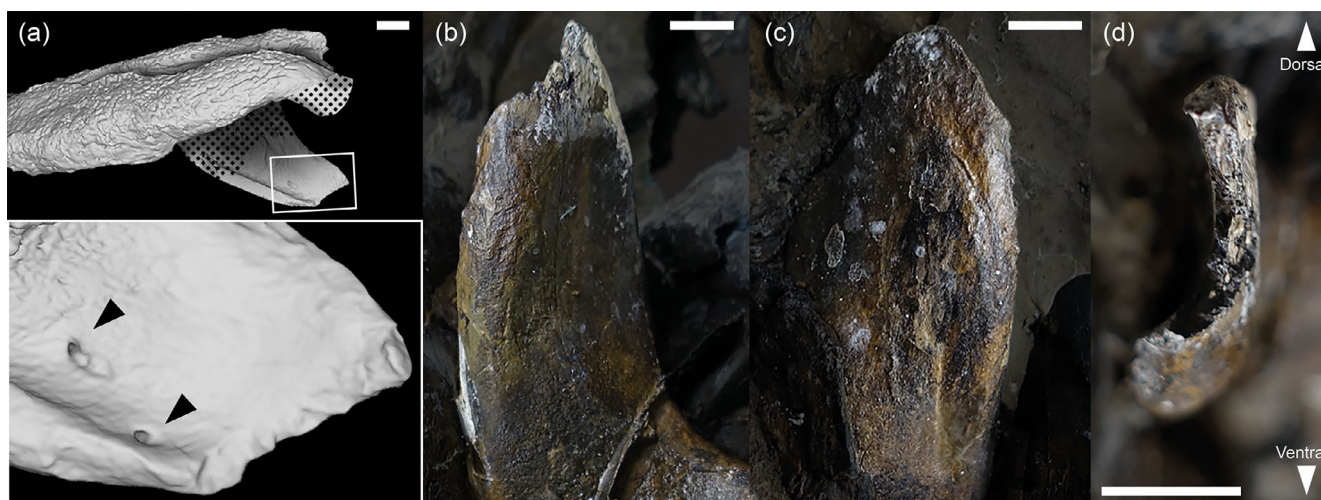


FIGURE 7 (a) surface rendering of the right pterygoid in lateral view (top), detail of the distal lateral surface (bottom). Black arrows highlight the lateral foramina. Ventromedial view of the left (b) and right (c) pterygoid flange; note the striated surface on the distalmost portions. (d) posteroventral view of the left distal pterygoid; note the vertical development of the process. Dotted areas in (a) represent inferred bone surfaces not isolated through segmentation. Scale bars = 10 mm (a), 5 mm (b, c, d).

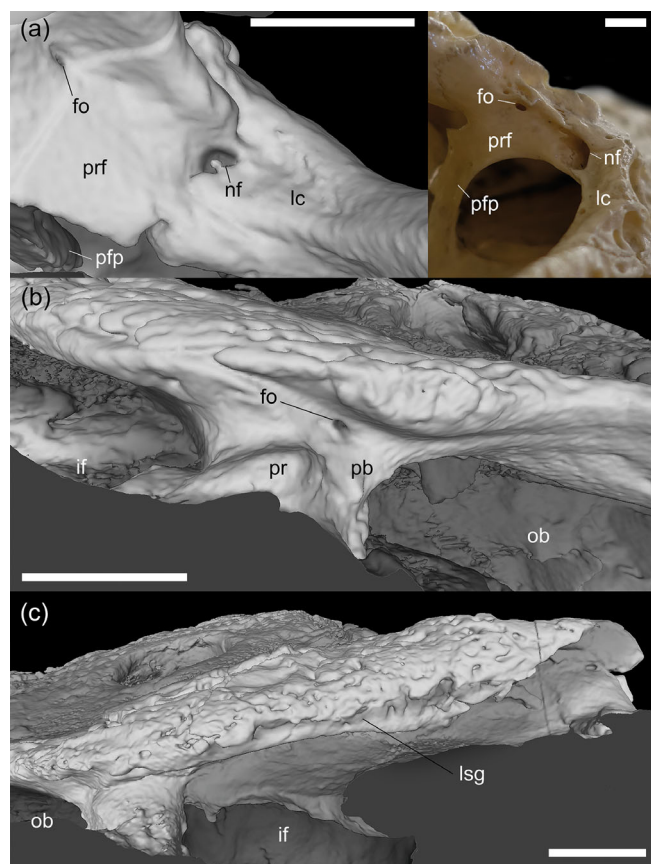


FIGURE 8 (a) anteromedial margin of the right orbit (contact area between lacrimal and frontal) in MCSNT 57248 (left) and modern *Caiman* sp. (right), with visible nasolacrimal foramen and upper portion of the prefrontal pillar. (b) detail of the right postorbital bar of MCSNT 57248 in lateral view. (c) detail of the lateral margin of the left squamosal and upper portion of the infratemporal fenestra. Scale bars = 5 mm (a), 10 mm (b, c). fo, foramen; if, infratemporal fenestra; lc, lacrimal; lsg, lateral squamosal groove; nf, nasolacrimal foramen; ob, orbit; pr, protuberance; pb, postorbital bar; prf, prefrontal; pfp, prefrontal pillar.

The orbital dorsomedial margins are upturned from the level of the frontal/lacrimal, but this relief might have been increased by the dorsoventral collapse of the frontal. The interorbital distance ratio is about 0.39, which is narrower than in *A. iberoccitanus* (0.46) but aligns with average crocodylian proportions. According to Rio and Mannion (2021), the largest values usually exceed 0.5, although this ratio is quite large for *Acynodon*. Comparatively smaller taxa like *Bernissartia fagesii* reach values as small as 0.17.

On the anterior wall inside both orbits, the nasolacrimal foramen is visible and not particularly large relative to the orbit size, closer to the widest portion of the orbit. This possibly neotenic trait is also seen in juveniles of modern crocodylians (Cerio & Witmer, 2022; Figure 8a).

In the left orbit, on the surface of the lacrimal just lateral to the nasolacrimal foramen, at least two smaller aligned neurovascular foramina are preserved. At least one rostrally oriented foramen is preserved on the surface of the prefrontal forming the anteromedial wall inside both orbits, medial to the nasolacrimal foramen, likely housing a minor vessel from the ophthalmic circulation.

The frontal is rostrocaudally elongated with a diamond-shaped anterior process intersecting the nasals, anterior to the orbits. It forms the medial margin of the orbits and the anteromedial margins of the supratemporal fenestrae. The sutures with the postorbitals are recognizable as symmetrical S-shaped grooves/cracks on the skull table, while the contacts with the prefrontals are difficult to establish but may correspond to symmetrical ornament-like grooves (Figures 2a and 4a). On its ventral surface, a low *crista cranii frontalis* visible on the right side delimits a shallow olfactory tract canal, which is mostly hidden by the palatal bar. The descending processes are more developed mediolaterally than dorsoventrally.

3.2.7 | Postorbital

The postorbital forms the posterior margin of the orbit, the anterolateral margin of the supratemporal fenestra, and partially overhang the infratemporal fenestra. The contact with the frontal appears S-shaped, while the dorsal sutures with the squamosals are nearly unrecognizable on both sides. On the lateral wall of the right supratemporal fenestra, an obliquely Z-shaped sulcus probably represents the suture between the postorbital and squamosal. The postorbital bars are short and stout, and more than 50% of their vertical expansion is seemingly formed by the postorbital. They are slightly antero-posteriorly expanded and elliptical in cross-section, with a slight protuberance on their lower dorsolateral surface (Figure 8b). A small foramen is preserved on the anterodorsal area of the right postorbital bar. As in *A. iberoccitanus*, the infratemporal fenestra is smaller than the orbit and proportionally very short. The ratio between the rostrocaudal length of the fenestra and the overlying skull table is between 0.2 and 0.3. The fenestra is roughly triangular, with the pointier left one probably more representative of the undeformed morphology.

3.2.8 | Squamosal and parietal

The supratemporal fenestrae are teardrop-shaped and slightly more elongated than wide, being more subcircular than in *A. iberoccitanus* (Figure 4a). The less

deformed right one has a length-width ratio of ~ 1.2 , while in *A. iberoccitanus* the same ratio is ~ 1.5 . The supratemporal fenestrae are also smaller than in *A. iberoccitanus*: in the latter, they occupy a little more than 40% of the anteroposterior length of the skull table, while in *A. adriaticus*, they occupy around 30%. Both supratemporal and anteromedial fossae are present, but their extensive visibility might be due to the fragmentation of the neurocranium. Inside the right supratemporal fenestra, the relatively large orbitotemporal canal seems to be preserved and devoid of matrix. On their internal medial wall, a shallow temporo-orbital groove (Bona et al., 2013) is preserved, and inside the left supratemporal fenestra, the parietal seems perforated by one or two tiny foramina. The parietal, alongside the entire skull table, is slightly concave. The slightly dorsally concave profile of the skull in occipital view is likely due to dorsoventral compression and collapse of the neurocranium (Figure 3a).

A straight horizontal groove running on the lateral walls of the supratemporal fenestrae represents the dorsal contact between the squamosal and quadrate. The posterolateral processes of the squamosals are well-developed and latero-ventrally oriented, contacting the paroccipital processes and quadrates. A faint groove merges with the dorsal ornamentations on the lateral margins of the squamosals overhanging the otic recess (Figure 8c), likely representing the dorsolateral squamosal groove for the insertion of the external ear flaps. Although somewhat less developed than in living eusuchians, this feature is present in other hylaeochampsids (e.g., *Hylaeochampsia vectiana*; Clark & Norell, 1992) but not in *I. makadui*, making *A. adriaticus* intermediate between the two conditions.

The otic recess is anteroposteriorly elongated, and the presence of matrix and dorsoventral compression makes further consideration of its deeper morphology impossible. Anteriorly, the dorsal and ventral margins of the squamosal over this structure are subparallel. The parietals are firmly fused (the sagittal keel is located where the suture would be) and appear as a single trapezoidal element, with its anterior contact with the frontal being completely unrecognizable. The lateral sutures with the squamosals are visible as posterolaterally oriented straight lines (Figures 2a and 4a).

3.2.9 | Supraoccipital, otoccipital, and basioccipital

Just posterior to the sagittal keel of the parietal, a thin crack separates a posterior medial bulge from the rest of the skull table (Figures 2a and 4a,d). This posterior

element can be identified as a relatively large, crushed supraoccipital, which contributes to the posterior skull table as in *Iharkutosuchus makadui* and extends mediolaterally for more than half of the parietal's mediolateral width. Its shape approximates a low and wide rhombus with a rugose prominence on its posterior vertical surface. In dorsal view, the posterolateral tuberosities are indistinguishable from the rest of the surface; there is no clear distinction between the medial and lateral occipital protuberances. This element is visibly compressed and located between the putative post-temporal fenestrae, preserved as small arched fissures. Their margins are formed dorsolaterally by the parietal, medially by the supraoccipital, and ventrally by the otoccipitals.

The otoccipitals (single element corresponding to fused exoccipital and opisthotic, sensu Kuzmin et al., 2021) are large, vertically oriented, and barely visible in dorsal view. The paroccipital processes are identifiable, flaring laterally under the squamosal prongs but barely reaching the same width as the medial quadrate hemicondyles. Under the left paroccipital process, the contact between the exoccipital and quadrate is visible, not reaching the articular surface of the medial hemicondyle as in *H. vectiana* and *I. makadui* (Rio & Mannion, 2021) (Figure 9a). A pit under the left paroccipital process, between the left exoccipital and the medial surface of the quadrate, probably represents the cranio-quadrate passage (CN VII) (Figure 9a). Under the arched process of the left paroccipital process and lateral to the occipital condyle, the metotic foramen is preserved as a relatively large, bisected pit. The metotic foramen houses cranial nerves IX–XI and relative vascularization, with the smaller medial foramen housing cranial nerves X and XI, and the larger lateral one housing IX and the sympathetic nerve (Bona & Desojo, 2011; Iordansky, 1973; Kuzmin et al., 2021). Based on available museum specimens, its shallowly bisected configuration seems closer to that observed in mature crocodylids rather than in alligatorids (Figure 10b,c), although this observation might be biased by the small sample size of comparative specimens.

A very small hypoglossal foramen (passage of cranial nerve XII) is visible, located medially close to the metotic foramen and lateral to the occipital condyle; a second one is probably present, but taphonomic damage makes its clear identification difficult. Ventral to the metotic foramen on the left side, the lateral carotid foramen is preserved as a subcircular pit. It seems closer to the metotic foramen than is seen in most crocodylians, almost resembling the “gavialoid” configuration (sensu character 126 of Rio & Mannion, 2021). Ventral to the supraoccipital and medial processes of the exoccipitals lies the dorsoventrally collapsed *foramen magnum*, with the

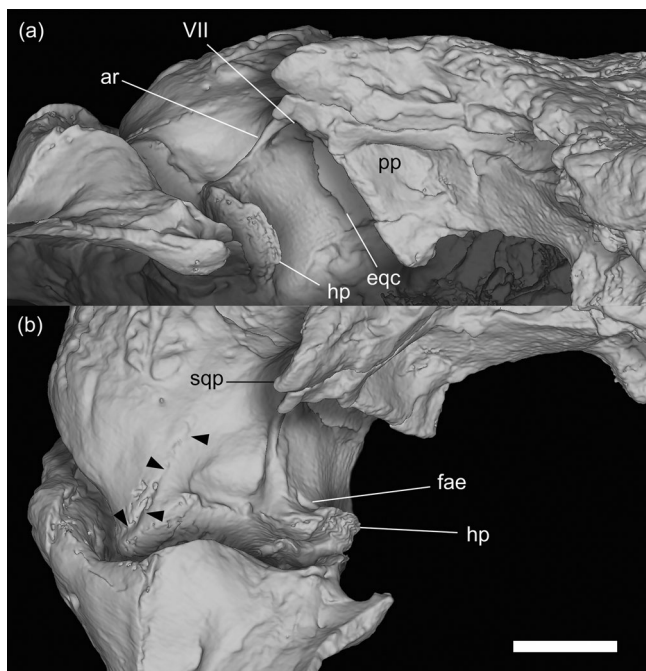


FIGURE 9 Detail of the left occipital area and quadrate of MCSNT 57248 in posteromedial (a) and dorsal (b) view. Black arrows highlight the contact between quadratojugal and quadrate. Scale bar = 10 mm. ar, ascending ridge of the quadrate; VII, Foramen for the 7th (facial) cranial nerve – cranioquadrate passage; eqc, exoccipital–quadrate contact; fae, foramen aereum; hp, hooked pathological process; pp, paroccipital process; sqp, squamosal prong.

underlying occipital condyle being the only recognizable structure of the basioccipital. The dorsoventral compression and overlying matrix completely hide the basisphenoid. The occipital condyle is medially furrowed (Figure 10a) and similar in shape to that of other living and extinct eusuchians, but proportionally very small. The ratio between the mediolateral width of the condyle and that of the skull in occipital view is around 0.07. In comparison, the same ratio is ~ 0.13 in *I. makadui*, ~ 0.15 in *A. iberoccitanus*, ~ 0.1 in *H. vectiana*, ~ 0.1 in *O. tetraspis*, 0.1 in *Tomistoma schlegelii*, 0.1 in *Caiman crocodilus*, 0.12 in *A. mississippiensis*, and 0.16 in young *Crocodylus* sp.

3.2.10 | Jugal and quadratojugal

The jugals of *A. adriaticus* are anteroposteriorly elongated and mediolaterally expanded elements. Together with the quadratojugals, they correspond to the widest region of the skull. The dorsolateral surface of the jugals is deeply ornamented and has a subhorizontal orientation, similar to other taxa with relatively small eyes and flat skulls such as *A. mississippiensis* and *C. latirostris*. Small foramina are preserved on the medial surface of the bone anterior to the postorbital process, but no foramen is present dorsally at the base of the postorbital bar. The posteroventral jugal foramina are not distinguishable

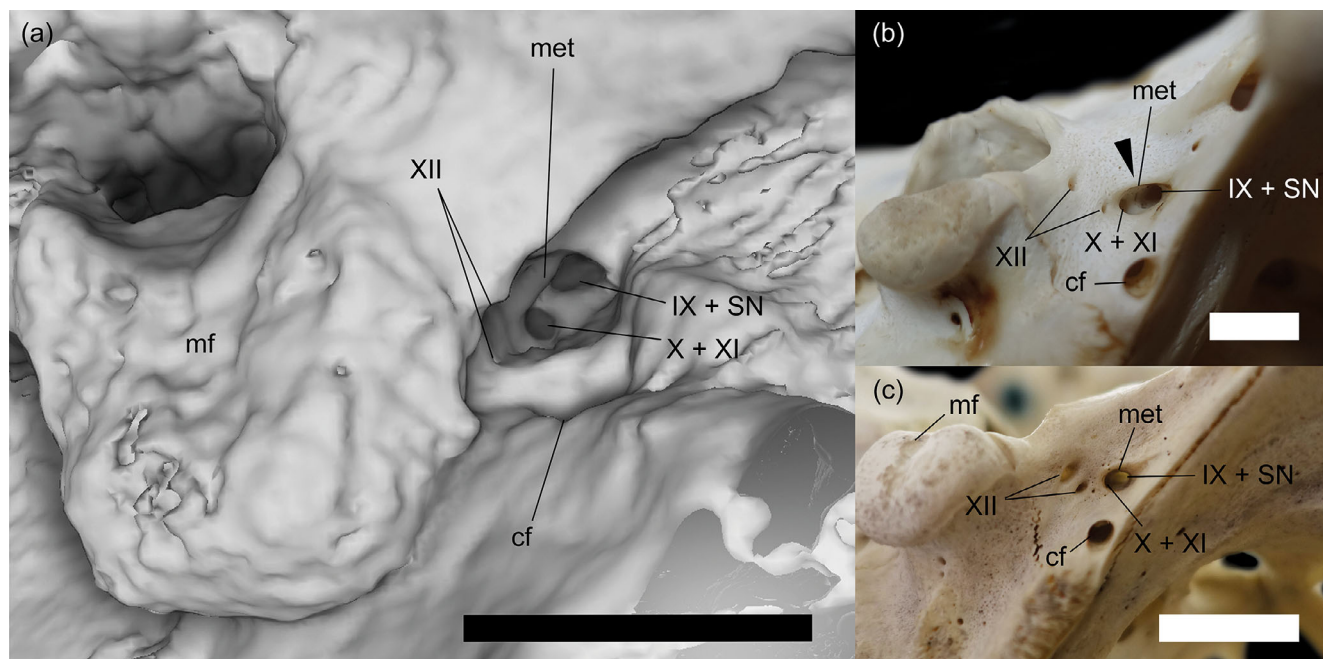


FIGURE 10 Detail of the occipital condyle and foramina in MCSNT 57248 (a), *Crocodylus* sp. (b) and *Alligator mississippiensis* (c). Scale bars = 5 mm (a, b), 20 mm (c). cf, lateral carotid foramen; IX, foramen for the 9th (glossopharyngeal) cranial nerve; met, metotic foramen; mf, medial furrow; SN, foramen for the sympathetic nerve; X, foramen for the 10th (vagus) cranial nerve; XI, foramen for the 11th (accessory) cranial nerve; XII, foramina for the 12th (hypoglossal) cranial nerve.

from the superficial foramina on the labial surface of the whole skull. Small foramina posterior to the last left alveolus are consistent with the morphology of jugal foramina but seem to perforate the posterior process of the maxilla rather than the anterior portion of the jugal. The ventral jugal arch is likely deformed due to dorsoventral compression: its ventromedial concavity would have originally been reflected in lateral view.

The dorsal profile of the jugal appears gently arched or continuous with the dorsal margin of the lower temporal bar, but a clear dorsal eversion just lateral to the post-orbital bar indicates a step-like convexity separating the orbit and the infratemporal fenestra. The contact with the quadratojugal is not clearly recognizable on both sides of the skull but seems to precede the posterior corner of the infratemporal fenestra (the latter being formed by the quadratojugal). The laterodorsal surface of this element clearly sports ornamentations, and the medial expansion forming the posterior edge of the infratemporal fenestra is smooth and elongated (Figures 2a and 4a). As reported by Delfino et al. (2008), the mediadorsal extent and contacts of this bone are difficult to establish, as the posterior margin of the infratemporal fenestra seems damaged, and sutures are not visible. The absence of the *spina quadratojugal* may therefore be a taphonomic artifact. The posterior process of the quadratojugals does not take part in the lateral quadrate condyle, remaining instead slightly more laterally offset (Figure 9b).

3.2.11 | Quadrate

The quadrates are short and wide (~23 mm), occupying approximately 36% of the maximum mediolateral width of the skull in occipital view (Figure 4). They are subparallel in orientation and extend more posteriorly than the occipital condyle. Both quadrates are fused with the quadratojugals, with a shallow groove marking the suture. Due to compression and damage, the otic portion of the quadrate is scarcely visible. The ventral surface of the quadrate is not exposed, but a muscle attachment scar is visible in the section through CT slices (Figure S4b). A pronounced protuberance on the anteroventral surface of the quadrate, likely homologous with muscle scar “A” of Iordansky (1964) and thus corresponding to the origin of the *m. adductor mandibulae posterior*, is known in *I. makadii* (Ösi, 2008; Ösi & Weishampel, 2009) and *Hylaeochampsa vectiana* (Clark & Norell, 1992). *A. iberoccitanus* also has a similar but less developed muscle insertion crest in the same area (Ösi, 2014). A comparable protuberance with rough texture on the ventral surface of the quadrate is reported in

Pietraroiasuchus ormezzanoi (Buscalioni et al., 2011), suggesting its presence as a common trait among hylaeochampsids. In *A. adriaticus*, this protuberance seems less developed than in *Iharkutosuchus* and *Hylaeochampsa*.

The quadrate has two condyles, separated by a well-defined groove, with the lateral one being larger. The medial condyle occupies about 36% of the mediolateral expansion, the lateral one about 50%, and the remaining space is represented by the intercondylar groove. The orientation of the joint is perpendicular to the rostrocaudal axis of the skull, as in *A. iberoccitanus* and most other crocodylians. The hooked process on both medial condyles, once considered a diagnostic character, likely represents craniomandibular joint arthritis, consistent with hyperossifications produced by similar pathological conditions in modern eusuchians (Holliday & Sellers 2024, personal communication).

Considering the diagenetic deformation, the articular surface of the condyles is roughly at the same level or slightly above the occlusal plane. The surface of the bone dorsal to the condyles features a deep subcircular pit aligned with the intercondylar groove, medially delimited by a sharp ascending ridge from the medial condyle terminating at the contact with the squamosal prong. This contact, previously reported as potentially pathological, likely represents genuine morphology given the smooth state of the bone and similar structure fragmentation on the right side. A similar but less developed structure is present in *A. iberoccitanus*. The left quadrate preserves a relatively small *foramen aereum* on the mesiodistal side of this ridge, just dorsal to the medial condyle's hooked process (Figure 9b), while it is not visible on the right quadrate.

3.2.12 | Dentary, angular, and surangular

The mandible is slightly posteriorward shifted and articulated in firm occlusion. The anterior half is visibly crushed against the palate, with the rami slightly medially rotated. However, the mandible in *I. makadii* and *A. iberoccitanus* is not significantly different, suggesting that despite the compression, the overall morphology is better preserved than the crushed skull. At roughly half the mandible length, the rami shows mediolateral torsion, becoming almost vertically oriented. They are both very tall and mediolaterally thick, producing a massive morphology as in *Iharkutosuchus*.

Each dentary has at least 16 alveoli, with the posterior ones being medially offset from the lateral margins of the jaw, similar to *A. iberoccitanus* and *I. makadii*. The external mandibular fenestrae are completely closed, and the oblique slit on the lateral surface of the left

hemimandible, revealed by tomographic scanning, represents a preparation artifact. None of the sutures between the dentary, angular, and surangular on the lateral surface are recognizable, and the ornamentation, especially on the posterior portion, is extremely developed. The inferior surface of the mandible under the craniomandibular joint is smooth, indicating a lateral insertion of the *m. pterygoideus ventralis*.

The symphysis is slightly open dorsally, visible through the naris and incisive foramen (Figure 5b). The ventrolateral surface is covered with foramina, some of considerable size. A row of larger labial foramina likely runs parallel to the dentigerous margin, visible posteriorly on the left side due to occlusion and matrix. As in living taxa, foramina on the lateroventral surface of the anterior mandible are aligned and often nested at the bottom of longitudinal grooves, merging with the keels and pits of the ornamentations. A portion of the Meckelian groove is visible at the posterior margin of the symphysis on the medial surface of the dentaries (Figures 11a,b and

S6). Both dentaries have a dorsoventral/oblique thickening and upward curve matching the position of the largest molariforms. The mandibular fossa is deep and oval-shaped, reaching the position of the last mandibular alveolus anteriorly (Figure 11a). The lateral walls of the mandibular fossae, comprising the medial surfaces of the surangular, angular, articular, and dentary, are submerged in matrix but may exhibit rugosity as indicated by CT slices (Figure S6). The dorsal mediolateral expansion of the surangular (Figures 11a and S6a) suggests a relatively wide dorsal surface for muscular insertions. The medial portion of the angular forming the inferior rim of the fossa has thick margins. The caudal intermandibular foramen is visible (although slightly hidden by the pterygoids) on both sides, displaying a rostrocaudally elongated oval shape. The exact contact between the angular and splenial is not identifiable. The coronoid is unrecognizable even by tomographic means, but the general morphology of the mandible suggests its presence dorsal to the caudal intermandibular foramen, possibly

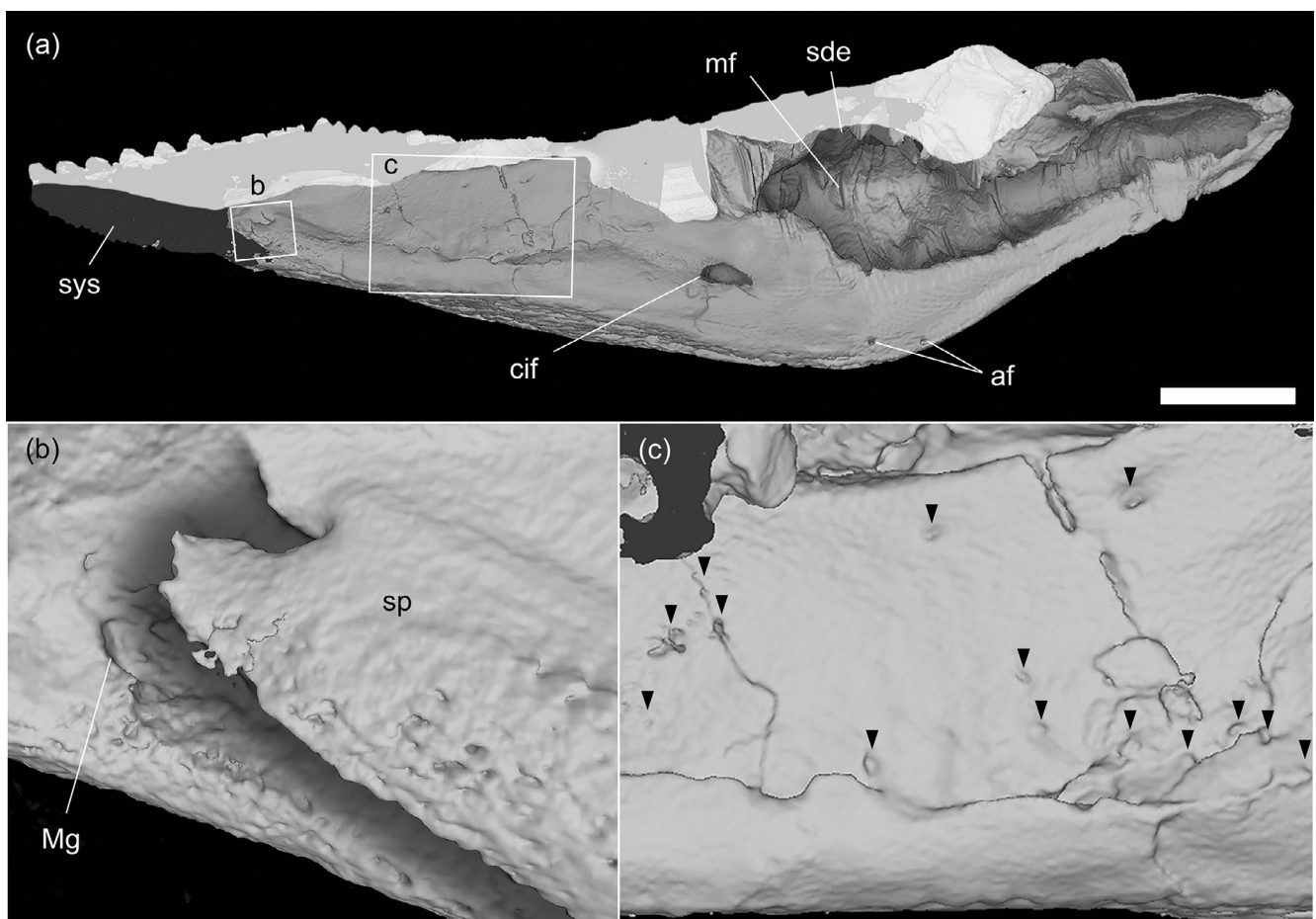


FIGURE 11 Medial view of the right hemimandible of MCSNT 57248 (a) and details of the anterior process (b) and middle surface (c) of the splenial. Black arrows highlight the medial splenial foramina. Scale bar = 20 mm. af, angular medial foramina; cif, caudal intermandibular foramen; mf, mandibular fossa; Mg, Meckelian groove; sde, surangular dorsal expansion; sp, splenial; sys, symphyseal surface.

contributing to the anterior margin of the mandibular fossa (similar to *A. iberooccitanus* and most other eusuchiaans; see Bona et al., 2022). The angular and surangular extend posterior to the tip of the retroarticular process, with the surangular also participating in the lateral rim of the articular glenoid cavity.

3.2.13 | Splenial

The splenials are clearly recognizable through direct observation and tomographic scans (Figure 11a). They are elongated and relatively thick, extensively fractured especially at their dorsal margins where they were crushed against the palate. They constitute most of the medial surface of the mandible, as in most crocodylians. The inferior suture with other bones appears as a shallow groove separating the lateroventral ornamented surface from the mediodorsal smooth one. The symphyseal processes are pointy and slightly disarticulated, ending close to the symphysis but not participating in it (Figure 11b). The most anterior tip of the symphyseal processes is roughly at the level of the 8th or 9th dentary alveolus. Small foramina randomly perforates the splenial surface, with two larger and aligned ones near the dorsal margin of the bone under the suborbital fenestrae (Figure 11c). No larger intermandibular *foramen oralis* is recognizable. Although the splenial likely forms the anterior margin of the caudal intermandibular foramen, its posterior surface is very undefined and its contacts with the coronoid and angular are not recognizable.

3.2.14 | Articular

The exact contact between the articular and the angular/surangular on their medial surface is not clearly visible. On the lateral side, the contact is relatively well preserved: dorsally, the suture with the surangular is slightly inset from the lateral rim of the glenoid fossa. At the border between the glenoid cavity and the retroarticular process, the suture remains slightly offset from the lateral edge and continues to the posterior tip of the retroarticular process (Figure 12). Ventrally, the contact runs along the inferior edge of the mandible. The dorsal surface of the articular on the retroarticular process is slightly lower than the lateral rim made by the surangular and has a caudolaterally oriented saddle-like convexity. Medially, the margin of the retroarticular process is broken on the left side but better preserved on the right, showing a thickened medial rim.

Ventrally, the entire retroarticular process has a deep concavity for the volumetric insertion of the

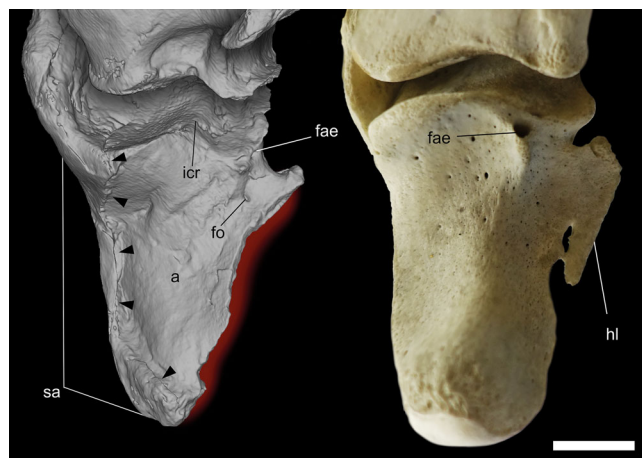


FIGURE 12 Detail of the articular and retroarticular process in dorsal view of MCSNT 57248 (left) and pathological *Alligator mississippiensis* (right). Black arrows highlight the contact between articular and surangular. Scale bar = 10 mm. a, articular; fo, foramen; fae, foramen aereum; hl, pathological hyperossified lamina; icr, intercotylar ridge; sa, surangular.

m. pterygoideus dorsalis, almost continuous with the more anterior mandibular adductor fossa. An anteroventrally oriented spine is preserved at the anteromedial corner of both retroarticular processes. These unusual projections are asymmetrical and show slight thickening and a rougher surface at their tips, likely representing pathological hyperossification of the *m. pterygoideus dorsalis* aponeurosis (Holliday & Sellers 2024, personal communication; Figure 12). Medial to these projections and caudomedial to the medial articular cotyles is a short dorsally directed spine, which usually encases or marks the position of the *foramen aereum*. On the right articular, no foramen is clearly identifiable, while on the left, the *foramen aereum* is located medially to the dorsal projection. Two additional foramina are present slightly more caudally, at the base of the anteriorly projected spine, with other smaller foramina scattered over the retroarticular dorsal surface.

The glenoid surface has a tall posterior bulge and expands medially over the underlying vacuity as a bony shelf. The glenoid cavity has two asymmetrical cotyles (the lateral one being larger) separated by a well-developed intercotylar ridge, matching the quadrate condyles. The glenoid cavity is slightly more rostrocaudally elongated than the quadrate condyle's articular surface, with proportions comparable to those in living crocodylians. As on the quadrate medial condyle, the medial margin of the glenoid surface bears a matching bony lamina, comparable to pathological bone morphologies in living samples.

3.2.15 | Premaxillary and maxillary dentition

The premaxilla contains five teeth per side, and the maxilla on the left side has 10 observable teeth. The total number of teeth on each side of the jaw is 18, with five premaxillary teeth (P1–5) and 13 maxillary teeth (M1–13; Figure 13a,c). Due to plastic deformation, teeth M4–13 are positioned obliquely labiolingually, with maximum inclination at M6–M8 under the collapsed maxillary margin. The premaxillary and the first six maxillary teeth share a similar morphology (Figures 14 and 15). Their

crowns are chisel-like, mesiodistally bicarinate, and compressed labiolingually. The labial surface is convex, while the lingual surface is slightly concave, with the labiolingual constriction lessening toward the base, giving an incisiform appearance. The apices are blunt, being slightly pointier in P1 and P2 and more rounded laterally in subsequent teeth. The enamel has fine, anastomotic apicobasal wrinkles (Figures 14b and 15a), and the carinae edges are smooth, without the false serrations seen in other crocodylians. The roots are notably developed, often more than twice the crown height, with a

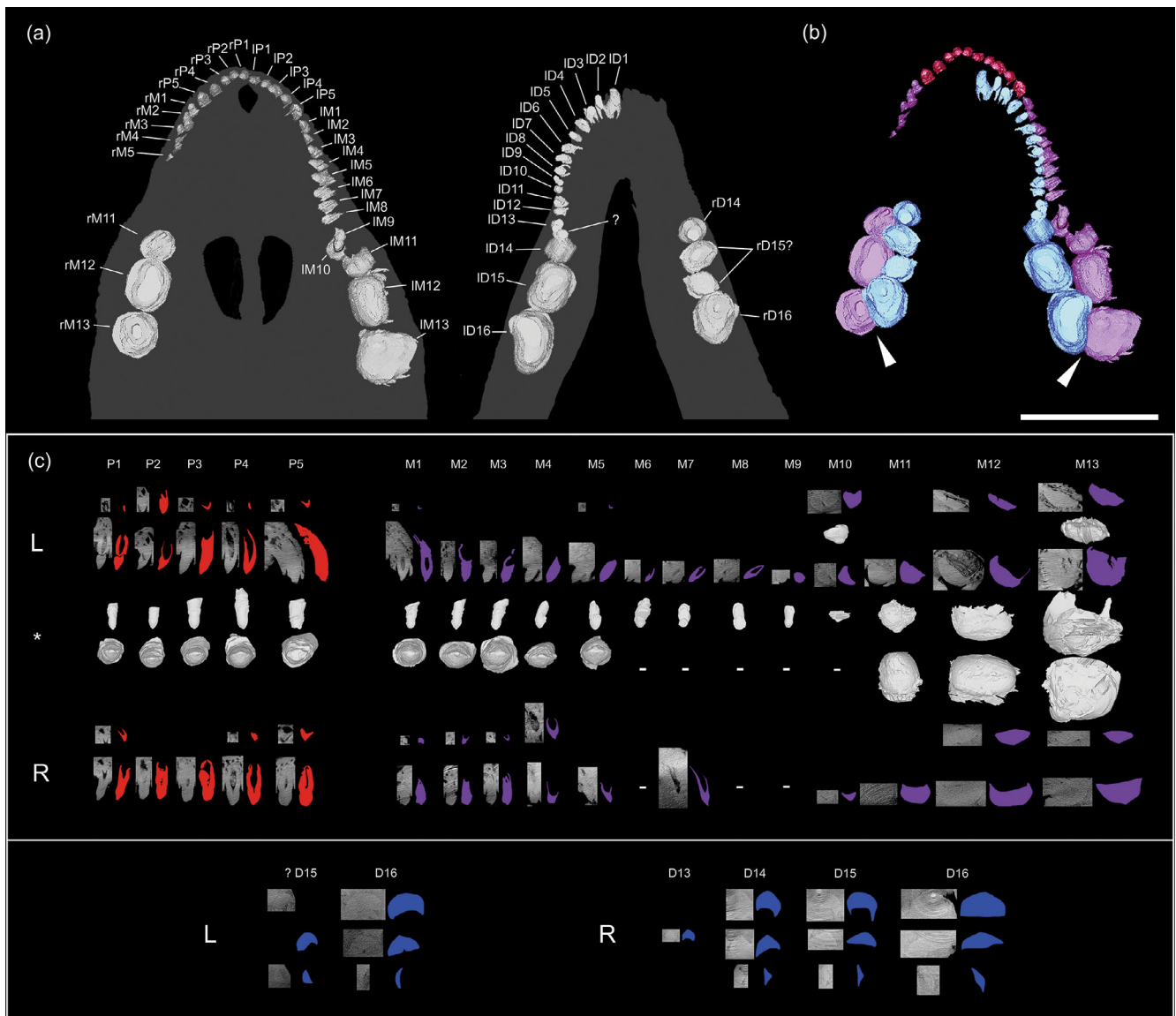


FIGURE 13 Upper (left) and lower (right) articulated dentition of MCSNT 57248 in occlusal view (a). Surface rendering of the occluding dentition as preserved (b). Note that both upper and lower teeth are here represented in occlusal view. (c) table with every clearly 3d-isolated tooth of the upper dentition and lower molariforms, with highlighted outline from the CT images. Of the upper left hemiarch, the labial and occlusal surface renderings of each well-preserved tooth are shown (*). Premaxillary teeth in red, maxillary teeth in purple, and dentary teeth in blue. White arrows in (b) highlight the partial tooth-on-tooth occlusion between molariforms. Scale bar = 50 mm. D, dentary tooth; l, left, M, maxillary tooth; P, premaxillary tooth; r, right.

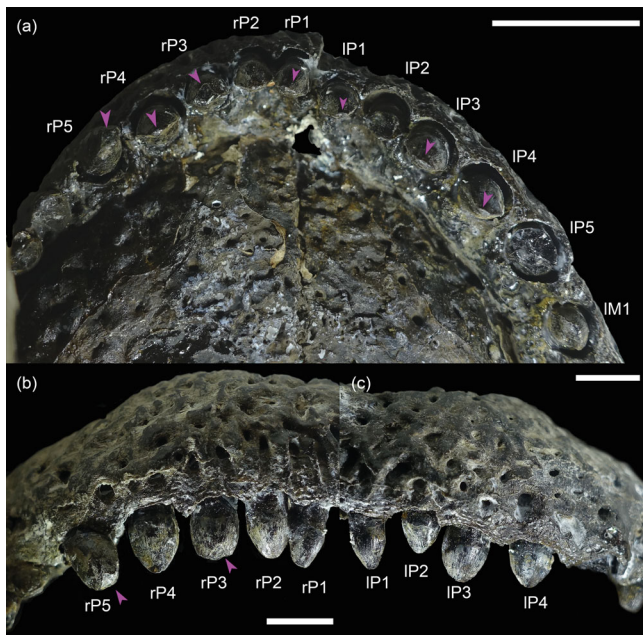


FIGURE 14 Occlusal (a) and labial (b, c) views of MCSNT 57248 premaxillary teeth. Purple arrows highlight apical wear facets. Note the palatal occlusal pits in (a). Scale bars = 10 mm (a), 5 mm (b, c). I, left; M, maxillary tooth; P, premaxillary tooth; r, right.

pronounced constriction at the base. P5 is the largest anterior tooth, while M6–M8 are the smallest. M9 is displaced horizontally over M10 and partly hidden by the collapsed maxillary margin (Figures 15b and 16a). It exhibits a transitional morphology between the anterior teeth and posterior bulbous molariforms, with a short, subconical crown adorned with apicobasal wrinkles transitioning to a rugose apex. The exposed root surface is smooth (Figure 16a).

Replacement teeth are present in every premaxillary alveolus except for the right P2 and P3 (Figure 13c). Among non-molariform maxillary teeth, replacement teeth are identified in M1 and M5 on the right side and M1–M5 on the left side. These successional teeth are mostly in early developmental stages, with only the left P2 and right M4 being more advanced. Morphologically these teeth resemble those of *Acynodon iberoccitanus* or *Iharkutosuchus makadii* and resemble the incisive teeth of some mammals or durophagous sparid fishes (Figure S5). Apical wear is visible in rP1, rP3, rP4, rP5, IP1, IP3, and IP4, with wear facets oriented diagonally toward the labial side (Figure 14).

Four molariform teeth are located in the posterior region of the maxilla (M10–M13). They are not fully

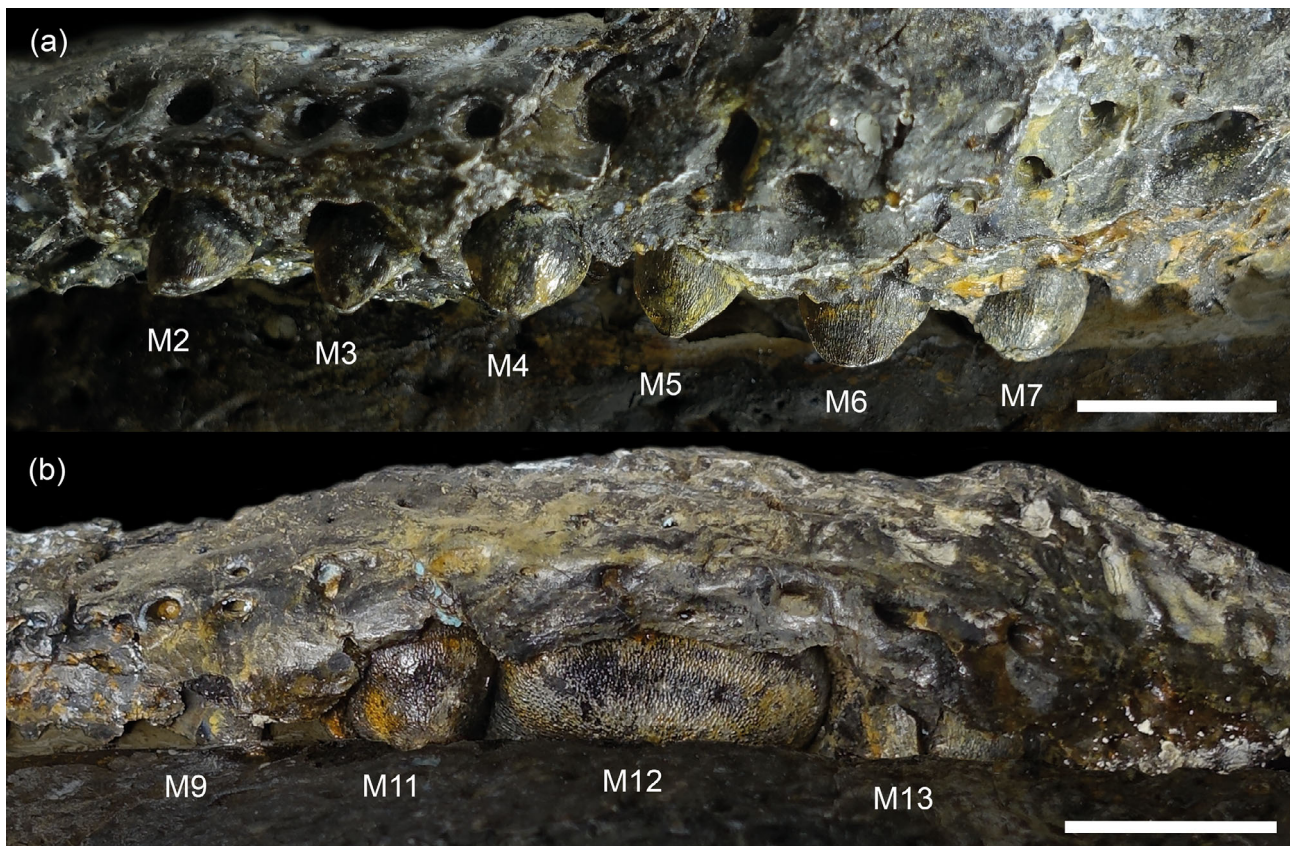


FIGURE 15 Lateroventral view of MCSNT 57248 left maxillary teeth 2–7 (a) and 9–13 (b). Scale bars = 5 mm (a), 10 mm (b). M, maxillary tooth.

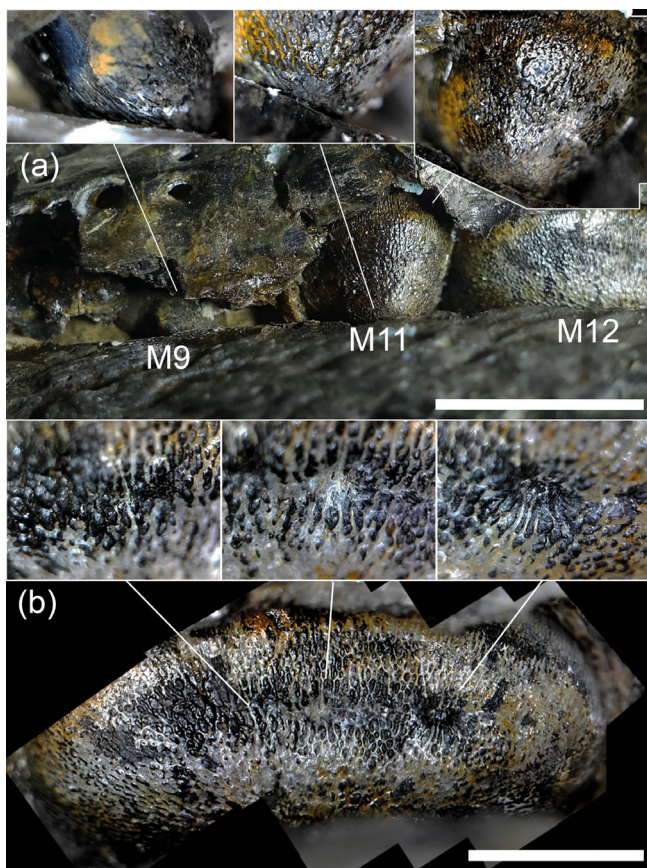


FIGURE 16 Detail of the exposed MCSNT 57248 maxillary molariforms M9–12 (a) and close-up of M12 (b) occlusal surface. Note the peculiar mesiodistally oriented pitting on M12. Scale bars = 10 mm (a), 5 mm (b). M, maxillary tooth.

visible due to the occluding mandible and the deformed maxillary bone (Figures 15b and 16). M10 on the left side is hidden but identified as larger than the anterior teeth yet the smallest molariform. A fully developed replacement tooth is deeper in the alveolus. The roots of M10 are short and thin. The right M10 is confirmed via CT data to have a similar crown shape. M11 shows a dramatic size increase and has a unique morphology with a labiolingually expanded, broad wedge shape, and a blunt conical apex. Its enamel shows deep apicobasal wrinkles at the base, becoming tuberculate near the apex (Figure 16a). The base of the crown is fractured, exposing thick enamel. The root is poorly preserved, and no replacement tooth is present. The right M11 shows more advanced apical wear. M12 on the left side is the best preserved, with a mesiodistal length of ~18 mm (Figure 16b). The crown is bulbous, with complex ornamentation and no wear traces. The root is thin and fractured, with a large, underdeveloped replacement tooth in the alveolus. The right M12 is similar but shows more advanced replacement tooth development. M13 on the

left side is fragmented but identified via CT data as the largest maxillary tooth. Its crown is subcircular/quadrangular, with thick enamel and dentin. The right M13 has a similar morphology but is slightly less expanded labiolingually. The upper dental row forms a U shape, widening at the posterior molariforms, influenced by deformation but resembling the dental arch of *Iharkutosuchus makadii*.

3.2.16 | Dentary teeth

Each dentary contains at least 16 teeth, with some uncertainty after ID13 due to overlapping elements (Figure 13a). The anterior teeth are subconical/chisel-shaped, followed by three large caudal molariforms. The first dentary teeth are best preserved, with poor conservation making it unclear if they show apical wear (Figure 5b). The first dentary teeth are procumbent, sub-horizontally oriented, and hook-like dorsally. The following 3–4 teeth are similar in morphology, suggesting strong procumbent orientation influenced by plastic deformation. The remaining non-molariform teeth are roughly similar in size and orientation, with progressively smaller roots and crowns up to D13/D14. The exact number of symphyseal alveoli is unclear, with a confusing spot at D13/D14 possibly indicating multiple elements or a fragmented tooth. Replacement elements are not identifiable.

The molariforms (D14–D16) are the largest dentary teeth, increasing in size toward D16 (Figure 13). Each molariform has a unique morphology. D14 is smaller, subspherical, with a quadrangular occlusal outline and an asymmetrical root. A large replacement tooth is present in the alveolus, with a second-generation replacement tooth lingually positioned. The right D14 shows the same morphology. D15 is twice the size of D14, elongated mesiodistally, with a regular surface and oval/rectangular occlusal outline. The root is poorly developed, with a large replacement tooth showing significant wear. The right D15 has two distinct elements in the same alveolus (Figures 13a and S6). This may be a product of taphonomic alteration or in situ fragmentation, but possibly even the result of an hyperdontia-like condition or anomalies during the replacement process [although there are no reported cases of true hyperdontia in crocodylians, reptiles are notoriously prone to oral pathologies and anomalies (Mehler & Bennett, 2003) and anecdotal and news reports of alveolar abscesses due to non-eruption of replacement teeth are common in captive crocodylians]. D16 is the largest, with a reniform occlusal outline and domed surface. The root is asymmetrical, with a large replacement tooth below. The right D16 is

mesiodistally less elongated, with a cusp on the antero-medial crown, and a large replacement tooth below. The unusual position of replacement teeth suggests specific replacement dynamics for these large posterior teeth. The lower dental arch forms a U shape, laterally expanded at the caudal molariforms, similar to the upper dentition and resembling *Iharkutosuchus makadai*. The lower teeth occlude lingually with the upper teeth, with molariforms showing partial tooth-on-tooth occlusion (Figure 13b).

3.2.17 | Description of the dentition in unrecovered in situ specimen

The new in situ fossil, pending proper preparation, offers insights into otherwise inaccessible elements. The coronal section reveals a clean cut of the skull and mandible, with sectioned molariforms and their replacements (Figure 17a). Comparisons with the holotype CT data allow rough identifications (Figure 17b). The dorsal margin is a sectioned skull roof with typical crocodylian ornamentations. A displaced tooth is diagonally cross-sectioned between the skull and mandible. The other sectioned teeth, identified as M12 or M13 and D16, match

the holotype CT data. The maxillary replacement tooth is angled, with a globular crown, ~8.4 mm high, and ~8.6 mm wide, with a maximum enamel thickness of ~1.8 mm at the apex. The maxillary functional tooth is ~13.5 mm wide and ~10 mm high, with root fragments and a total height of ~18 mm (Figure 17c). The dentary functional tooth is smaller, ~10.9 mm wide and ~5.5 mm high, with a D-shaped section and a maximum enamel thickness of ~0.6 mm. The replacement dentary tooth is of comparable size. A small vertically oriented enamel crescent near the replacement tooth indicates a second-generation replacement tooth (Figure 17d). The enamel and dentine in these teeth are consistent with the holotype CT data, showing detailed structure and replacement dynamics.

3.3 | Muscle insertions and musculoskeletal reconstruction

The skull of *A. adriaticus* (specimen MCSNT 57248) is well-preserved, allowing for detailed myological considerations (Figure 18). Extensive literature exists on crocodylian jaw musculature, detailing the morphology,

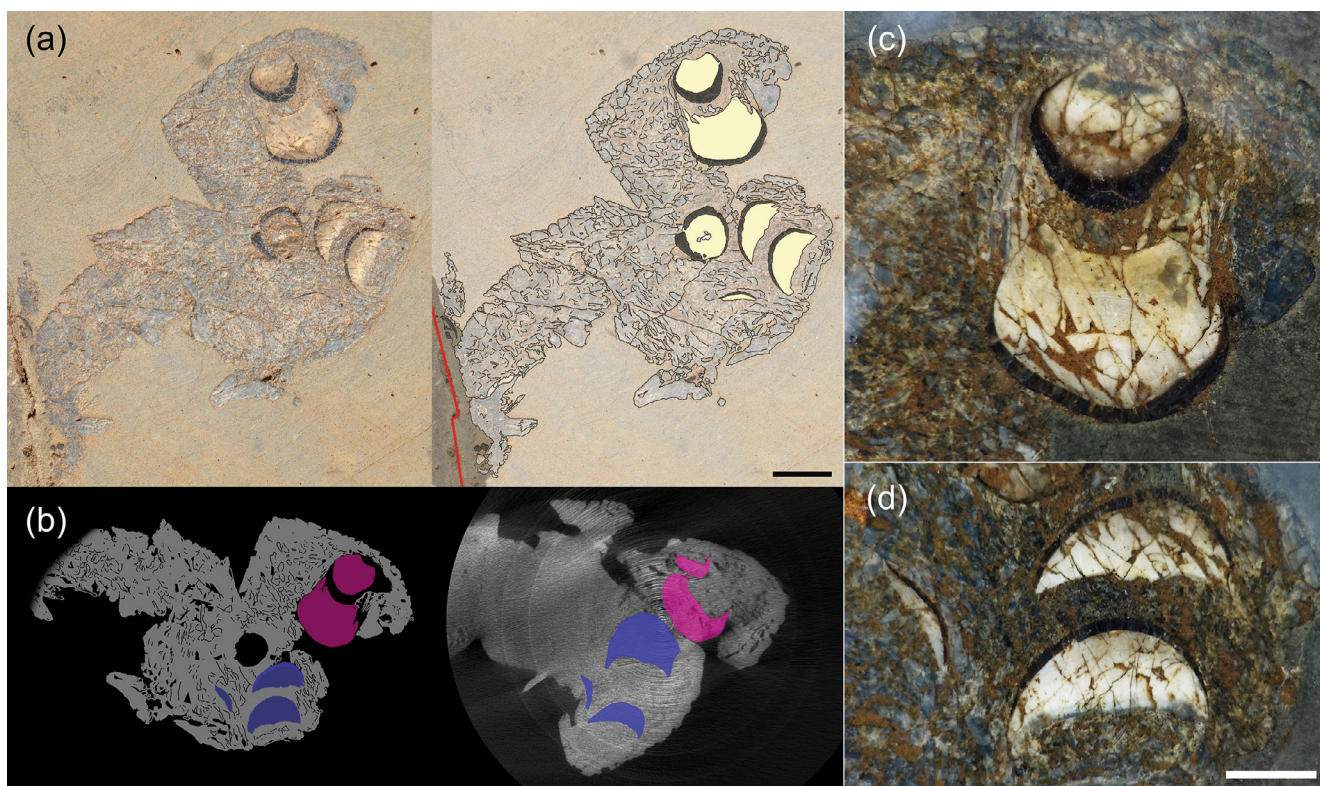


FIGURE 17 The uninventoried in situ sectioned skull. (a) photograph of the specimen (left) and superimposed interpretative drawing (right). The red line represents a fault. (b) comparison between the interpretative drawing of the specimen (left) and tomographic slice of MCSNT 57248 taken at a similar level (right). Dentary teeth are highlighted in blue, maxillary teeth are highlighted in purple. Closeup of the sectioned maxillary teeth (c) and dentary teeth (d). Scale bars = 10 mm (a), 5 mm (c, d).

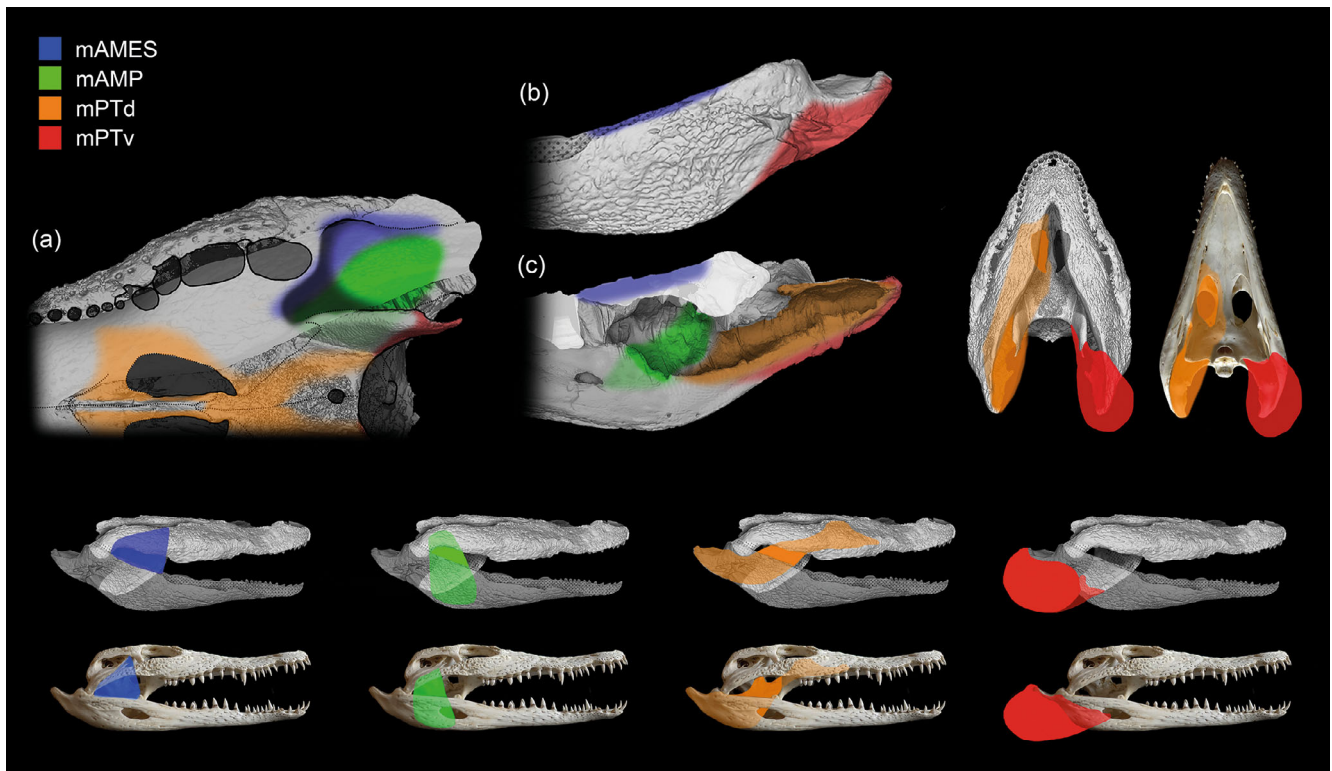


FIGURE 18 Schematic diagram of putative adductor muscle attachment areas of the skull (a) and mandible in lateral (b) and medial (c) view, and comparisons of hypothetical muscle volumes in *A. adriaticus* and a similarly sized *Crocodylus* sp. Only the four supposedly main adductors are represented, highlighted in coherent colors. Elements not to scale. mAMES, musculus adductor mandibulae externus superficialis; mAMP, musculus adductor mandibulae profundus; mPTd, musculus pterygoideus dorsalis; mPTv, musculus pterygoideus ventralis.

configuration, and functional implications across various taxa (e.g., Bona & Desojo, 2011; Busbey, 1989; Drongelen & Dullemeijer, 1982; Holliday et al., 2013; Holliday & Witmer, 2007; Iordansky, 1964; Sellers et al., 2022). The following considerations are mainly based upon Holliday and Witmer (2007), Holliday et al. (2013), and Sellers et al. (2022). The genus *Acynodon* has been previously discussed in the context of heterodont crocodylomorphs (Ösi, 2014), but notable distinctions exist between *A. adriaticus* and *A. iberoccitanus*, particularly in the mandible, secondary palate, pterygoid, and retroarticular processes, which likely influenced jaw musculature configuration.

Five muscles are particularly noteworthy in this context: *m. intramandibularis* (mI), *m. adductor mandibulae externus superficialis* (mAMES), *m. adductor mandibulae posterior* (mAMP), *m. pterygoideus dorsalis* (mPTd), and *m. pterygoideus ventralis* (mPTv). In modern crocodylians like *A. mississippiensis*, mI inserts into the Meckelian canal, extending anteriorly to the fifth—sixth posterior dentary alveoli or further (Holliday et al., 2013). However, in *A. adriaticus*, CT scans reveal that the mandibular rami were largely occupied by large inferior

molariform alveolar chambers, suggesting a thinner or significantly shorter mI, although the deep mandible may have allowed for compensatory vertical muscle development. The muscles mAMES and mAMP are the primary non-ptyerygoidean mandibular adductors in crocodylians. mAMES extends from the ventromedial surface of the quadrate and quadratojugal to the dorsal surface of the surangular, slightly protruding between the jugal–quadratojugal and the mandible. While a functional reduction of mAMES is proposed in *I. makadui* (Ösi & Weishampel, 2009), *A. iberoccitanus* has a large insertion area on the mediolaterally widened surangular, indicating a well-developed mAMES (Ösi, 2014). Similarly, *A. adriaticus* shows a widened surangular surface (Figures 18b,c and S4a), although the anteroposterior space for this muscle is limited due to the position of the crushing dentition near the jaw joint, akin to the modern molluscivore *Dracaena guianensis* (Dalrymple, 1979).

The mAMP, a voluminous adductor originating from the quadrate's anterior surface, extends deeper toward the surangular, angular, and articular, reaching the Meckelian fossa and contacting the *cartilago transiliens*. The deep posterior mandible in *A. adriaticus* likely

provided increased vertical attachment surface, with potential ventral shifts in muscle insertion areas due to the closure of the mandibular fenestra. This muscle configuration is similar to *Iharkutosuchus makadii*, which also lacks the mandibular fenestra (Ösi & Weishampel, 2009). Furthermore, *A. adriaticus* shows a likely protruding muscle scar on the quadrate's ventral surface (Figure S4b), likely corresponding to the origin of mAMP (Figure 18a). The pterygoideus muscles, mPTd, and mPTv, are the most important jaw adductors in both living and extinct crocodylians. mPTd originates from the anteromedial margins of the suborbital fenestrae and caviconchal area, the internal surface of the suborbital region and dorsal palate, attaching to the angular and articular surfaces and the retroarticular process via the posterior pterygoid tendon lamina superior (Holliday et al., 2013; Holliday & Witmer, 2007; Sellers et al., 2022). mPTv, originating from the pterygoid and its aponeurosis, wraps around mPTd and the retroarticular process, attaching to the ventrolateral surfaces of the articular and angular.

In *A. adriaticus*, the suborbital fenestrae and palatine bar suggest a more anterior mPTd insertion surface, with a narrow configuration for the anteromedial portion. The ectopterygoids, though partially hidden, may indicate ample insertion surface for mPTd's lateral fibers, similar to *Iharkutosuchus* (Ösi & Weishampel, 2009). The deep posterior mandible and elongated retroarticular processes in *A. adriaticus* suggest a large posterior insertion area for mPTd, with anomalous hyperossifications of the mPTd aponeurosis possibly due to mechanical loading and sustained use (Killian, 2022). The caudally arching pterygoids may have supported additional insertion area for mPTv, and the striated texture of the pterygoids' posterior process indicates strong tendinous attachment of the posterior pterygoid tendon lamina posterior.

The non-ornamented smooth surfaces on the ventrolateral side of the angular and the retroarticular process support the lateral insertion of mPTv (Figure 18b). Together with mPTd, mPTv would have been extremely developed, facilitating a powerful bite. This muscle arrangement is seen in *I. makadii*, where even mediolateral jaw movement was likely possible for processing a varied diet and allowed for independent hemimandible rotation due to an unossified symphysis (Ösi, 2014). In *A. adriaticus*, the symphysis is unfused, visible through the incisive foramen, but significant kinesis is unlikely given the taphonomic disarticulation observed in both fossil and modern crocodylians. The articular glenoid fossa in *A. adriaticus* is slightly longer than the quadrate's articular surface, with proportions similar to modern *Crocodylus* species, suggesting that the partial disarticulation observed in the fossil is not indicative of any significant

adaptation and can be replicated with modern osteological specimens.

4 | DISCUSSION

4.1 | Tooth replacement

All known crocodylomorphs exhibit plesiomorphic thecodont polyphyodonty, where new generations of teeth are continuously produced throughout an individual's lifespan within specialized thecae (alveoli). These teeth progressively migrate labially under the functional position, creating an asymmetrical resorption pit on the lingual side of the functional root (Juuri et al., 2013; Whitlock & Richman, 2013; Wu et al., 2013) (Figure 19a). Multiple generations of replacement teeth can coexist in the same socket, with up to six successional elements observed in *C. niloticus* (Pitman, 1931). Considering factors like adult size, the rate of size increase in successional teeth during ontogeny, and the average lifespan of modern taxa such as *Crocodylus* and *Alligator*, dental renewal can support the replacement of individual teeth up to 40–50 times (Poole, 1961). However, cases of edentulous senescent captive individuals and permanent tooth loss in wild specimens suggest that regenerative limits exist (Erickson, 1996b).

In the holotypic skull of *A. adriaticus*, notably, few of the anterior chisel-like teeth show underlying replacement teeth at advanced developmental stages. Additionally, the long, robust roots of most of these teeth are mostly intact and lack typically advanced resorption pits from growing successional elements. Conversely, nearly every molariform has at least one well-developed replacement tooth (Figure 13c). Some replacement teeth are slightly labially offset from the functional tooth axis, and the labiolingual asymmetry in erupted teeth roots likely represents physiological resorption on their lingual side. This suggests that the dental replacement dynamics in *A. adriaticus* were similar to those in living eusuchians. Successional posterior teeth in *A. adriaticus* are almost perfectly aligned below or above the functional elements, indicating a physical replacement process somewhere between the classical crocodylian linguo-labial migration and a vertical tooth succession akin to the palatine plate-shaped teeth of placodonts (Neenan et al., 2014; Pommery et al., 2021; Rieppel, 2001). This vertical replacement in Placodontia likely evolved due to space constraints from the large size and shape of their crushing teeth, a situation that seems comparable to tribodont neosuchians.

An intriguing feature in the two *A. adriaticus* specimens is the orientation of second-generation successional

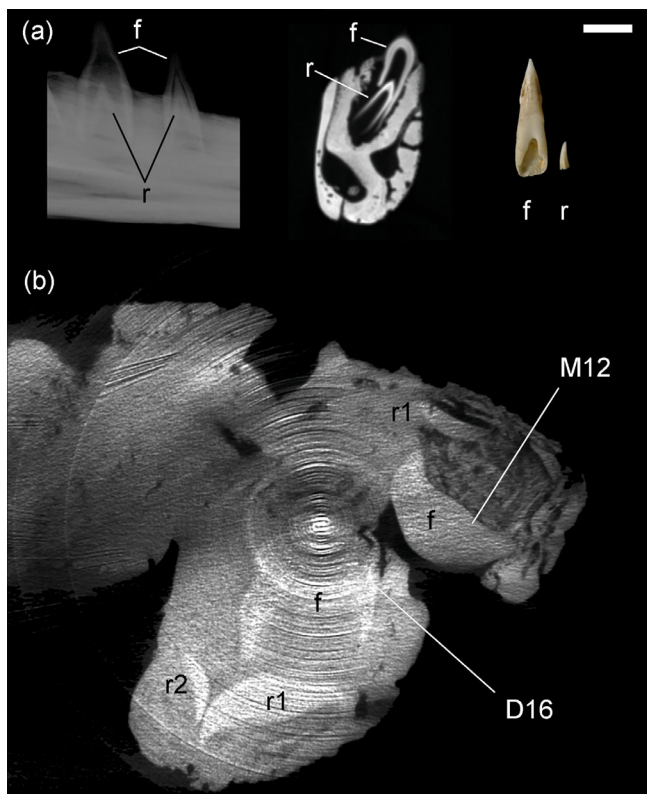


FIGURE 19 (a) Examples of replacement teeth position, dynamics, and shape in a portion of right *Crocodylus niloticus* hemimandible; lateral x-ray view of articulated functional and replacement teeth (left), CT cross-section of an alveolus containing both functional and replacement tooth (middle), extracted functional tooth and replacement element in lingual view (right). Note the triangular lingual resorption pit on the root of the functional tooth. (b) CT slice of the left side of MCSNT 57248 at the level of the larger molariforms (M12–D16) with brightened outlines of the preserved articulated dentition. Note the subvertical orientation of the second-generation replacement tooth of D16. Scale bar = 5 mm. f, functional; D, dentary tooth; M, maxillary tooth; r, replacement; r1, first generation replacement tooth; r2, second generation replacement tooth.

teeth of dentary molariforms D14, D15, and D16. Underdeveloped cusps are positioned lingually, deeply nested at the bottom of large alveolar chambers, and oriented diagonally in a subvertical position with the occlusal surface pointing labially. CT data in both left (D14–D16) and right (D15 and D16) dentaries of the holotype highlight this condition (Figures 13c, 19b), also observable in the in situ skull's D16. Typically, early developmental stages of teeth align similarly to the erupted element in the same alveolus. However, significant rotation of replacement teeth is known in non-tetrapod vertebrates, such as the Jurassic durophagous lepisosteiform *Scheenstia*, which exhibit up to 180° rotation during tooth development (Leuzinger et al., 2020).

Among thecodont sauropsids, unusual replacement teeth orientation is noted in durophagous taxa like placodonts, where the decay of soft tissue inside large alveoli allows smaller replacement teeth to move freely within the chambers (Neenan et al., 2014).

The consistency of the oblique orientation in *A. adriaticus* across multiple teeth and specimens suggests that this orientation is genuine rather than postmortem reorientation. In situ obliquely oriented successional molariforms, embedded in their original soft tissue, are also observed in CT scans of the dome-toothed savannah monitor *Varanus exanthematicus* and *Tiliqua scincoides* (The Deep Scaly Project, 2006a, 2006b), as well as in the osteologically prepared specimen of the small crocodylian *Ostelaemus tetraspis* (Ekdale, 2006). Though these species differ in tooth implantation and replacement dynamics and the mentioned teeth are mostly maxillary, the occurrence of unusually oriented successional crushing teeth in other taxa may indicate a more common, yet underreported, condition in species with enlarged molariform dentition. The oblique early growth of the large molariforms in *A. adriaticus* could have optimized space allocation, allowing for more efficient successional tooth production in a tight arrangement. This adaptation might have ensured that at least one mature crown was always present under the functional dentary molariform, with a third crown in earlier stages. This arrangement, reminiscent of that seen in placodonts, suggests both a higher replacement rate and a potential biomechanical role for the successional teeth as structural reinforcement elements before eruption.

Tooth replacement in polyphyodont taxa varies widely in functional and ontogenetic diversity, typically classified into sequential and alternate (Zahnreihen; Edmund, 1960) replacement patterns (Bertin et al., 2018; Whitlock & Richman, 2013). Sequential replacement involves contiguous teeth positions gradually moving along the jaw, while alternate replacement involves distinct waves replacing alternate teeth positions, ensuring adjacent teeth are not simultaneously in a precarious replacement state. Most amniotes exhibit different iterations of the alternate pattern, with replacement waves moving mesio-distally or disto-mesially. The replacement rate in extinct taxa is usually assessed by comparing the incremental lines of von Ebner in a functional tooth and its replacement tooth (Erickson, 1996a), or by comparing the developmental stages of all teeth undergoing replacement (Whitney & Sidor, 2019; Wu et al., 2021).

In the upper dentition of the scanned *A. adriaticus* holotypic skull, few advanced replacement elements are present among the chisel-shaped anterior teeth, while almost every molariform has at least one replacement element, with up to two generations of successional teeth

observed in lower molariforms. Modern eusuchians typically follow an alternate replacement pattern with an anteroposterior gradient, where posterior teeth are replaced less frequently than anterior ones (Cooper et al., 1970). In *A. adriaticus*, there is clear alternation in anterior replacement teeth without bilateral symmetry, with only two anterior teeth positions (left P2 and right M4) approaching replacement at the time of death. Every upper and lower molariform has at least one replacement element, suggesting a higher replacement rate and a different replacement pattern. An opposite pattern, seen in placodonts and the hylaeochampsid *Iharkutosuchus makadii* (Ösi, 2008), might represent shared adaptations among hylaeochampsids for processing hard or abrasive foods, potentially converging with durophagous sauropterygians.

4.2 | Durophagy and trophic palaeoecology of *a. adriaticus*

In living sauropsids, the occasional consumption of hard-shelled prey—especially terrestrial or aquatic mollusks—is common and widespread among clades, even in taxa without obvious durophagy-associated adaptations such as insectivorous squamates and herbivorous tortoises (Kosma, 2004; Thorn et al., 2019; Muscioni, personal observation, 2023). Slow-moving hard-shelled preys are often abundant, representing an easily exploitable resource in healthy ecosystems. However, relying on the consumption of hard items as a frequent food source is likely disadvantageous without specific anatomical specializations that help overcome the energetically costly processing of hard shells. True durophagous non-edentulous vertebrates actively consume hard and brittle food items through oral processing with specialized dentition, generally represented by enlarged, blunt, bulbous molariform teeth with crushing functions (defined as “tribodont” in the case of *Bernissartia* by Buffetaut & Ford, 1979) and robust skulls. In addition to tooth morphology, durophagy is associated with an adaptive complex of converging traits such as reduced tooth count and increased biting performance (e.g., *Dracaena guianensis*, Dalrymple, 1979; de Souza et al., 2021).

However, the evolution of such features should not necessarily be considered a signal of dietary preference. Among living durophages, true active specialization with almost exclusive mollusk ivory seems to be represented only by the teiid *Dracaena* spp., the dactyloid *Chamaeleolis* spp., and the scincid *Cyclodomorphus gerrardii*, with other possible candidates being other *Cyclodomorphus* species, *Tiliqua gigas*, *Eumeces schneideri*, the amphibaenians *Amphisbaena ridleyi*, and *Trogonophis wiegmanni*

(Berkovitz & Shellis, 2017; Herrel & Holanova, 2008; Kosma, 2004; Martín et al., 2013; Mesquita et al., 2006; Moran, 1979; Pregill, 1984; Sander, 1999; Schaerlaeken et al., 2012). Much more commonly, many living taxa with specialized durophagous dentition have generalist/opportunistic diets. Taxa such as *Tiliqua* spp. and adult teiids such as *Tupinambis teguixin*, *Salvator rufescens*, and *Salvator merianae* notoriously have omnivorous diets that include plant material, fruits, and arthropods in addition to mollusks (Kosma, 2004; Mercolli & Yanosky, 1994; da Silva et al., 2020). On the other hand, *Varanus niloticus*, *V. albigularis*, *V. exanthematicus*, and *V. olivaceus* are either opportunistic predators or omnivorous frugivores, with negligible direct observations of gastropod or crustacean consumption (Bennett, 1995, 2014; Sander, 1999; D'Amore, 2015; Muscioni, personal observation, 2023).

The generalist diet of seemingly phenotypically specialized animals is referred to as Liem's Paradox (Bouton et al., 1997; Golcher-Benavides & Wagner, 2019; Robinson & Wilson, 1998). Many resources are abundant and intrinsically easy to exploit, while others require specialized foraging traits to be consumed; morphological specializations allow strategic access to otherwise unexploitable resources while retaining the ability to forage for easier food items, thus broadening the feeding niche and enabling competition against true morphological generalists. Functional specialization may arise toward foods that are important only seasonally or during specific recurring environmental phases. When exposed to changes in competitive interactions and/or prey abundance and availability, this phenomenon may lead to true ecological specializations with active preferences: the aforementioned exclusive molluscivorous taxa are often nested in clades with generalist ecologies but shared morphological predispositions toward durophagy (e.g., *Dracaena* among generalist teiids *Salvator* and *Tupinambis*, *C. gerrardii* among other *Cyclodomorphus* species or generally in the Egerniinae together with *Tiliqua* spp. and *Egernia* spp., Thorn et al., 2019; *Chamaeleolis* among the generalist insular *Anolis*).

All living eusuchians might be considered opportunistic and generalist carnivores, with even longirostrine gavialoids such as *Tomistoma schlegelii* being able to occasionally prey on medium–large mammals, including humans (Grigg & Kirshner, 2015; Sideleau et al., 2022). Except for longirostrine taxa, all living crocodylians are heterodont with blunter posterior teeth whose degree of molariform morphology varies among species, reaching its maximum development in *Alligator* spp., *Melanosuchus niger*, *Osteolaemus* spp., and *Caiman latirostris*, the latter sometimes being effectively considered a molluscivore (Diefenbach, 1979; Ösi & Barrett, 2011). The diet of

most living crocodylians includes invertebrates, whose consumption is not abandoned even in mature individuals of large species (e.g., Silveira & Magnusson, 1999). Observed or suspected frequent consumption of mollusks and crustaceans is known in many living taxa (e.g., *Crocodylus mindorensis*, Brown et al., 2021; *Osteolaemus* spp., Pauwels et al., 2007; Brown et al., 2021; Smolensky et al., 2023; *Alligator* spp., Chen et al., 1985; Delany & Abercrombie, 1986; Rice, 2004; Berkovitz & Shellis, 2017; *Caiman latirostris*, Diefenbach, 1979; Borteiro et al., 2009; Ósi & Barrett, 2011; *Caiman crocodylus*, *Melanosuchus niger*, and *Paleosuchus* spp., Magnusson et al., 1987; Thorbjarnarson, 1993; Silveira & Magnusson, 1999; Horna et al., 2003). None of the living species, however, display the same level of durophagy-oriented heterodonty and molariform specializations as the much more diverse extinct taxa (e.g., the chelonivorous teleosaurid *Machimosaurus* spp., Young et al., 2014; bernissartiids, Buffetaut & Ford, 1979; Sweetman et al., 2014; hylaeochampsids, Delfino et al., 2008; Ósi, 2014; Jouve et al., 2017; basal alligatoroids such as *Allognathosuchus* spp., *Brachychampsia* spp., and others, Sullivan & Lucas, 2003; Ósi, 2014; *Bottosaurus* spp., Cossette & Brochu, 2018; the crocodyloid “*Crocodylus*” *bambolii*, Delfino & Rook, 2008; the South American *Gnatusuchus pebasensis*, *Kuttanacaiman iquitosensis*, and *Caiman wannlangstoni*, Salas-Gismondi et al., 2015; *C. brevirostris* and *Globidentosuchus brachyrostris*, Scheyer & Delfino, 2016). Both living and extinct non-herbivorous heterodont crocodylians likely shared a tendency toward a highly plastic generalized diet, and the presumedly durophagous adaptive traits need better contextualization.

With few exceptions, the enamel of durophagous teeth typically exhibits convergent microstructure between taxa, a finely ornamented surface, and increased thickness (Sander, 1999). The enamel ornamentation in durophages is usually represented by fine anastomotic wrinkling and apicobasal ridges/radial striae on both lingual and labial surfaces of the tooth (Figure S7). Superficial enamel wrinkling and rugosity may increase mechanical stress resistance, grip over preys, concentrate pressure in smaller punctiform areas, and progressively increase microfractures in brittle surfaces (Sander, 1999). Besides lateral ornamentation, the apex of durophagous teeth is usually characterized by increased thickness, internal orthodontine, and anastomosis of the apicobasal ridges converging into a more rugose surface, thus enhancing strength and wear resistance (Martín et al., 2013; Nobre & Carvalho, 2006). Although the sole presence or absence of apicobasal striae does not strictly correlate with durophagy (McCurry et al., 2019), its presence with anastomotic patterns and alongside apical rugosity indicates a significant functional signal. The

enamel thickness values of *A. adriaticus* measured on the sectioned specimen surpass those of living durophages and rank among the highest known in reptiles, alongside placodonts, the globidensine mosasaurs and durophagous ichthyosaurs—these often representing remarkably larger animals. Generally, the absolute average enamel thickness scales isometrically with skull length (Sellers et al., 2019). Comparing the maximum recovered enamel thickness relative to skull length of various sauropsids with known (or inferred) trophic ecology suggests that this relationship remains true between different carnivorous or herbivorous taxa, but durophage values remain consistently higher and less influenced by absolute skull size (Figure 20). Big skulls with large teeth are intrinsically preadapted for crushing hard food items due to the isometrically thicker enamel and absolute larger size of the adductor musculature, lightening the selective pressure for proportionally thicker enamel. An overall increase of skull size represents a recurring strategy to aid in hard-shelled food processing (Schaeerlaeken et al., 2012). *Acynodon* is small for modern crocodylian standards, but comparable in size to the other hylaeochampsids, globidontians, basal neosuchians such as the bernissartiids and the modern durophagous squamates *Dracaena* spp. and *Varanus* spp.; yet the absolute enamel thickness values are closer to those of specialist molluscivores, in which they also rank as some of the highest observed, suggesting that a strong selection acted toward high stress-load capacity and low failure risk in molariform teeth. The values of known and putative durophages with more generalist ecologies are proportionally high, but not as high as those of more specialized taxa.

In morphofunctional terms, the skull traits of *A. adriaticus* clearly indicate a specialization for durophagy. The dentition of *A. adriaticus* includes heterodont non-carinated teeth with wrinkled enamel and converging apicobasal ridges (Delfino & Smith, 2012). The ornamentation pattern, enamel thickness, wear stages and replacement dynamics suggest an actively durophagous trophic ecology. Like living durophagous sauropsids, it likely mainly relied on the frequent consumption of hard-shelled prey such as aquatic and terrestrial mollusks and crustaceans, presumably integrating with a certain degree of generalism including arthropods, small vertebrates and possibly plant material.

4.3 | Palaeoecological context

Large-scale biotic phenomena of the latest Cretaceous might be crucial in the ecological contextualization of *A. adriaticus*, in addition to the controversial paleoenvironmental data of the VdP (see the Supporting Information).

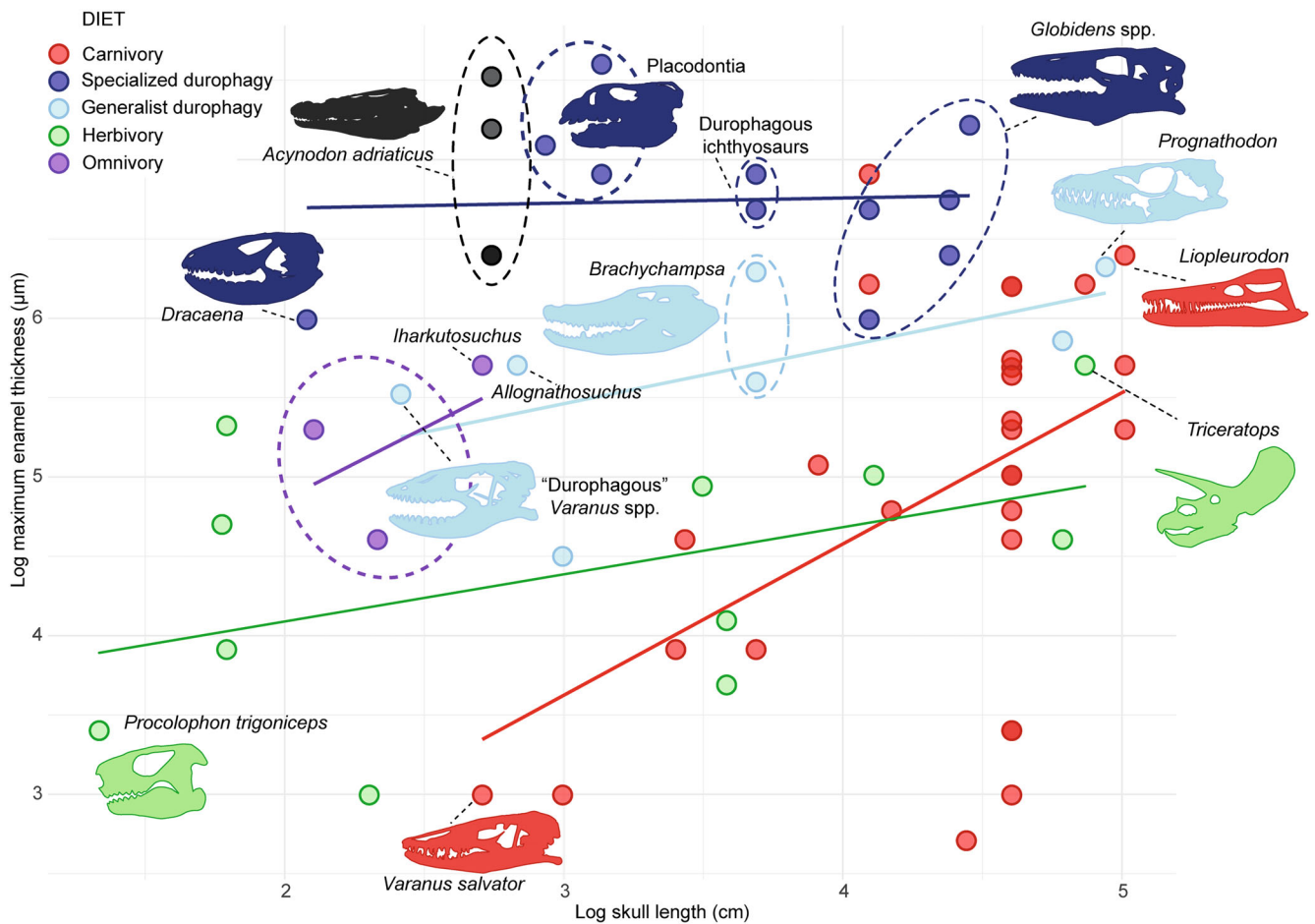


FIGURE 20 Regressions of maximum recovered enamel thickness (y) and skull length (x) of various living and fossil amniotes falling in the main trophic ecologies (carnivory, herbivory, omnivory, generalism—oriented durophagy and specialized durophagy). Note that regression lines of all categories show strong positive relationships between absolute skull size and tooth enamel thickness, while in specialized durophagous taxa, the regression line is almost horizontal. Data from *Acynodon adriaticus* (black) falls in the same range of highly specialized durophages such as *Dracaena* and durophagous sauropterygians. See Supporting Information for the raw dataset, references for visualized data values and specimens, and a raw plot with names for every represented taxon. R^2 values: Carnivory = 0.225, specialized durophagy = 0.0024, generalist durophagy = 0.321, herbivory = 0.204, omnivory = 0.242.

For instance, during the Santonian, a combination of biotic and abiotic factors led to a peak in the speciation rate of freshwater gastropods in Europe (Neubauer et al., 2021; Neubauer & Harzhauser, 2022). The reasons behind this phenomenon are probably linked to an increase in marginal humid habitats, the overall geographic fragmentation of the European archipelago, and the pervasive diffusion of angiosperms following the Cretaceous Angiosperm Terrestrial Revolution (Benton et al., 2022). These conditions were followed by a general fall in global sea level during the Campanian, which increased the available emerged land surface, mitigating the effect of intraspecific competition and increasing available freshwater habitats. The outcome of these phenomena was a peak in European freshwater gastropod diversity during the early Campanian, around 81 million years ago (Neubauer & Harzhauser, 2022). Other freshwater invertebrates likely benefited from

these conditions. Given the re-evaluation of the VdP biota as lower-middle Campanian, between 81.5 and 80.5 million years ago (Chiarenza et al., 2021), the known time range of *A. adriaticus* is consistent with a regional-scale, highest freshwater molluscan diversity.

Analogies to this pattern are represented by the rapid repeated evolution of durophagous sauropterygians following the Early Triassic invertebrates' diversification (Huang et al., 2020) and the durophagous caimanines of the Miocene Pebas megawetland ecosystem (Salas-Gismondi et al., 2015). In the latter, a peak in proto-Amazonian molluscan diversity and abundance coincided with the radiation of small-sized brevirostrine caimans with variably durophagous/molluscivorous trophic ecologies, such as *Gnatusuchus pebasensis* and *Kuttanacaiman iquitosensis*. Although no precise data are available to infer molluscan taxa sympatric with

A. adriaticus, both gastropods and bivalves are known from the VdP, representing ~1% of the fossil material (this value most likely represents an underestimation prior to a complete revision). Traces covering entire slab surfaces, on the contrary, may be coherent with bottom littering by a large amount of gastropod fecal pellets, as observable in modern shallow freshwater and brackish habitats with relatively high densities of grazing gastropods. Their underrepresentation is not surprising, as it was likely influenced both by sampling biases during quarrying and by taphonomic phenomena linked to carbonate shell preservation in acidic waters. Other potential prey more represented at the site (~3% of the fossil material) are relatively large undescribed decapods; however, the correlation between cancrivory and durophagous traits is less clear.

Although it is not possible to determine whether crocodylomorphs were year-round residents or seasonal/occasional frequenters, nor if the site acted as a tetrapod trap, it is common for small extant eusuchians to disperse on land from nearby source populations to rely on ephemeral, smaller pools and streams, where they can be more competitive than their larger sympatric counterparts.

5 | FINAL REMARKS

Among Hylaeochampsidae, *Acynodon adriaticus* stands out as one of the most complete and better-preserved taxa, represented by articulated cranial and postcranial material and multiple specimens. Integrating traditional investigation methods with micro-CT highlighted previously overlooked or poorly visible features and significant internal structures. This revision of both holotypic and new skull material provides a refined understanding of cranial and dental features, yielding invaluable information on the anatomy and palaeoecology of this taxon.

Life history traits of the holotypic skull are detectable. Specimen MCSNT 57248 represents a mature to senescent individual, with hyperossification of dermal bones and highly developed ornamentations. At the time of death, the individual had accumulated various pathologies. In addition to the healed fracture callus on the left ulna mentioned by Delfino et al. (2008), the peculiar spines and bone curtains of the quadrate-articular and retroarticular regions likely represent symptoms of jaw joint arthritis. Two separate teeth arising from the same alveolus in the left dentary, if not an artifact of taphonomy, may represent a case of hyperdontia-like condition. Micro-CT processing allowed for the description of previously undetectable morphologies of the skull osteology, providing a baseline for future taxonomic revisions and phylogenetic analyses of Hylaeochampsidae.

The palaeoecological inferences rendered possible by the anatomical assessment are immediate. Most representatives of Hylaeochampsidae seem to have exhibited an array of unusual dental adaptations, with possibly omnivorous, herbivorous, and durophagous taxa. *Acynodon adriaticus* appears to have one of the most obvious and dramatic sets of durophagous traits. The brevirostrine and massive skull have biomechanical adaptations for enhanced performance of the adductor muscle complex, hinting at a powerful bite and high stress-load capacity—a key recurring trait of the molluscivory adaptive complex (de Souza et al., 2021). The anatomy of the quadrate-articular joint suggests stiff and stable orthal mobility. The specialized dentition lacks caniniform teeth as in other hylaeochampsids, featuring anterior chisel-like teeth and posterior hypertrophic globular molariforms with extremely thick enamel. Some of these are very similar in shape to those of bernissartiids but exhibit more complex ornamentations, with unique mesiodistally oriented pitting, and may sport diagnostical morphologies. Teeth rows occlude in an overbite on the anterior half of the jaw, with partial tooth-on-tooth occlusion between posterior molariforms. Preserved successional teeth support a specialized accelerated replacement rate of the molariforms and a lower rate for the anterior incisiforms, a feature shared with *Iharkutosuchus makadui* and a possible converging trait with placodonts. Dentary molariforms underwent an unusual oblique/subvertical early mineralization phase, possibly as a solution to space constraints. Quantitative analysis based on dental and cranial morphofunctional traits places *A. adriaticus* among other extinct and extant molluscivore specialists. The relatively small orbit size suggests very small eyes (see Cerio & Witmer, 2022) and consequently reduced eyesight, a common phenomenon in aquatic tetrapods inhabiting scotopic environments.

Among eusuchians, *A. adriaticus* was probably one of the most specialized toward durophagy, benefiting from the rise of invertebrate diversity triggered by biotic turnovers and habitat oscillations of the Upper Cretaceous. This small crocodylomorph was likely a slow forager of shallow benthic environments in turbid or densely vegetated waters, gripping mollusk shells and large arthropod exoskeletons with its finely wrinkled teeth and crushing them with increased muscular power and optimized lever configuration. As with modern durophages, *A. adriaticus* probably relied on relatively intense intra-oral food processing, an unusual strategy for living crocodylian standards but consistent with the inferred ecologies of other Cretaceous hylaeochampsids such as *Iharkutosuchus makadui*. Many extinct crocodylians sported stronger heterodonty compared to living taxa, with a combination of anterior caniniform and conical bicarinate teeth followed

by posterior crushing molariforms. This was traditionally interpreted as a dietary specialization toward durophagy, but it probably arose as a competitive advantage, permitting a widened prey selection that may have included abundant hard-shelled invertebrates as a seasonal or strategic food source. However, very few taxa display an unambiguous set of derived traits compatible with true specialization as in *A. adriaticus*, which, alongside *G. pebasensis*, should be considered a morphofunctional model for drawing ecological inferences from fossil crocodylians.

AUTHOR CONTRIBUTIONS

Marco Muscioni: Conceptualization; investigation; writing – original draft; methodology; visualization; writing – review and editing; software; data curation; formal analysis. **Alfio Alessandro Chiarenza:** Supervision; writing – review and editing; visualization; software; investigation; validation; formal analysis; methodology; writing – original draft. **Diego Bladimir Haro Fernandez:** Software; methodology; data curation. **Diego Dreossi:** Supervision; methodology; writing – review and editing; software; data curation. **Flavio Bacchia:** Funding acquisition; resources; methodology. **Federico Fanti:** Supervision; funding acquisition; writing – review and editing; project administration; visualization; resources; validation; writing – original draft; methodology.

ACKNOWLEDGMENTS

Data and results presented in this study were possible thanks to the Accordo Quadro Agreement between Università di Bologna (Dip. BiGeA), Università di Trieste (Dip. di Matematica e Scienze della Terra), Museo Civico di Storia Naturale di Trieste, ISPRA, Elettra Sincrotrone, and ZOIC s.r.l. The authors thank all those involved in the ongoing research project on the VdP site. The Soprintendenza Archeologia, Belle Arti e Paesaggio del Friuli-Venezia Giulia facilitated the study of the vertebrate remains from the VdP (prot. 3289 dd. 22/02/2022 to F. Fanti). We wish to thank Dott.ssa S. Bonomi, Dott.ssa P. Ventura, and Dott.ssa P. Loccardi (SABAP Friuli Venezia Giulia) for their commitment to scientific research related to the VdP site. We thank Dr. P. Fasolato, Dr. F. Locci, and all the staff of the Museo Civico di Storia Naturale in Trieste for granting access to VdP material in their care. Special thanks are reserved to Dott.ssa D. Arbulla for her irreplaceable assistance, and Dr. K. Milocco for his support and help during specimen inspections. We are grateful to the staff of the TomoLab (Elettra Sincrotrone) for their hospitality and support. We are indebted to G. Bacchia and Zoic s.r.l. for disclosing personal and historical information on the site. We also thank M. Sartori and the Comune di Duino Aurisina

for granting access to the site. We are thankful to Prof. C. Holliday and Dr. K. Sellers for sharing their expertise on the topic. We also thank A. Lazzarini and P. Pagliarulo for providing access to specimens of living taxa and direct ethological observations, L. Casoni for sharing veterinary considerations, and A. Formoso for sharing her graphical expertise. Special thanks go to Dr. F. M. Rotatori and Prof. M. Delfino for their professional advice and shared opinions about this work. We are grateful to the Editor Dr. L. Kerber, Dr. F. Barrios, and an anonymous reviewer for valuable comments that significantly improved this manuscript. We acknowledge that images of specimens provided in this study are courtesy of Soprintendenza ABAP FVG-MiC (art. 108, co.3 D. Lgs 42/2004s.m.i). Open access publishing facilitated by Università degli Studi di Bologna, as part of the Wiley - CRUI-CARE agreement.


FUNDING INFORMATION

Marco Muscioni PhD project is funded by NextGenerationEU—Piano Nazionale di Ripresa e Resilienza (PNRR)—XXXIX cycle, STVA University of Bologna, and ZOIC s.r.l. Alfio Alessandro Chiarenza was supported by the Royal Society Newton International Fellowship (NIF\R1\231802). Diego Bladimir Haro Fernandez PhD project is funded by the Programma Operativo Nazionale (PON).

ORCID

Marco Muscioni  <https://orcid.org/0000-0002-1429-0294>

Alfio Alessandro Chiarenza  <https://orcid.org/0000-0001-5525-6730>

Diego Bladimir Haro Fernandez  <https://orcid.org/0009-0007-5266-1459>

Diego Dreossi  <https://orcid.org/0000-0003-2727-1145>

Federico Fanti  <https://orcid.org/0000-0002-2961-8301>

REFERENCES

- Andrews, C. W. (1913). On the skull and part of the skeleton of a crocodile from the middle Purbeck of Swanage, with the description of a new species (*Pholidosaurus laevis*), and a note on the skull of *Hylaeochampsia*. *Annals and Magazine of Natural History*, 8(11), 485–494. <https://doi.org/10.1080/00222931308693345>
- Bennett, D. (1995). *A little book of monitor lizards*. Viper Press.
- Bennett, D. (2014). The arboreal foraging behavior of the frugivorous monitor lizard *Varanus olivaceus* on Polillo Island. *Biawak*, 8, 15–18.
- Benton, M. J., & Clark, J. M. (1988). Archosaur phylogeny and the relationships of the Crocodylia. In M. J. Benton (Ed.), *The phylogeny and classification of the Tetrapods, volume I: Amphibians, Reptiles, and Birds* (pp. 295–338). Clarendon Press.
- Benton, M. J., Wilf, P., & Sauquet, H. (2022). The angiosperm terrestrial revolution and the origins of modern biodiversity. *New Phytologist*, 233(5), 2017–2035. <https://doi.org/10.1111/nph.17822>

- Berkovitz, B., & Shellis, P. (2017). *The teeth of non-mammalian vertebrates*. Elsevier. <https://doi.org/10.1016/B978-0-12-802850-6.00009-6>
- Bertin, T. J. C., Thivichon-Prince, B., LeBlanc, A. R. H., Caldwell, M. W., & Viriot, L. (2018). Current perspectives on tooth implantation, attachment, and replacement in Amniota. *Frontiers in Physiology*, 9, 1630. <https://doi.org/10.3389/fphys.2018.01630>
- Bona, P., Degrange, F. J., & Fernández, M. S. (2013). Skull anatomy of the bizarre Crocodylian *Mourasuchus nativus* (Alligatoridae, Caimaninae). *The Anatomical Record*, 296(2), 227–239. <https://doi.org/10.1002/ar.22625>
- Bona, P., & Desojo, J. B. (2011). Osteology and cranial musculature of *Caiman latirostris* (Crocodylia: Alligatoridae). *Journal of Morphology*, 272, 780–795. <https://doi.org/10.1002/jmor.10894>
- Bona, P., Fernandez Blanco, M. V., Ezcurra, M. D., von Baczko, M. B., Desojo, J. B., & Pol, D. (2022). On the homology of crocodylian post-dentary bones and their macroevolution throughout Pseudosuchia. *The Anatomical Record*, 305(10), 2980–3001. <https://doi.org/10.1002/ar.24873>
- Borteiro, C., Gutiérrez, F., Tedros, M., & Kolenc, F. (2009). Food habits of the broad-snouted caiman (*Caiman latirostris*: Crocodylia, Alligatoridae) in northwestern Uruguay. *Studies on Neotropical Fauna and Environment*, 44(1), 31–36. <https://doi.org/10.1080/01650520802507572>
- Bouton, N., Seehausen, O., & van Alphen, J. J. M. (1997). Resource partitioning among rock-dwelling haplochromines (Pisces: Cichlidae) from Lake Victoria. *Ecology of Freshwater Fish*, 6, 225–240. <https://doi.org/10.1111/j.16000633.1997.tb00165.x>
- Brochu, C. A. (2003). Phylogenetic approaches toward Crocodylian history. *Annual Review of Earth and Planetary Sciences*, 31, 357–397. <https://doi.org/10.1146/annurev.earth.31.100901.141308>
- Brochu, C. A., Parris, D. C., Grandstaff, B. S., Denton, R., & Gallagher, W. B. (2012). A new species of *Borealosuchus* (Crocodyliformes: Eusuchia) from the late cretaceous–early Paleocene of New Jersey. *Journal of Vertebrate Paleontology*, 32, 105–116. <https://doi.org/10.1080/02724634.2012.633585>
- Brown, J. C., Shirley, M. H., Yog-yog, A., van Weerd, M., Balbas, M. G., Tarun, B. A., & Siler, C. D. (2021). Use of diet and body condition assessments as intermediate indicators of translocation success in the critically endangered Philippine crocodile (*Crocodylus mindorensis*). *Aquatic Conservation: Marine and Freshwater Ecosystems*, 31(10), 2817–2829. <https://doi.org/10.1002/aqc.3700>
- Buffetaut, E., & Ford, R. L. E. (1979). The crocodylian *Bernissartia* in the Wealden of the Isle of Wight. *Palaeontology*, 22, 905–912.
- Busbey, A. B. (1989). Form and function of the feeding apparatus of *Alligator mississippiensis*. *Journal of Morphology*, 202(1), 99–127. <https://doi.org/10.1002/jmor.1052020108>
- Buscalioni, A. D., Ortega, F., & Vasse, D. (1997). New crocodiles (Eusuchia: Alligatoroidea) from the upper cretaceous of southern Europe. *Comptes Rendus de l'Académie Des Sciences*, 325, 525–530. [https://doi.org/10.1016/S1251-8050\(97\)89872-2](https://doi.org/10.1016/S1251-8050(97)89872-2)
- Buscalioni, A. D., Piras, P., Vullo, R., Signore, M., & Barbera, C. (2011). Early eusuchia crocodylomorpha from the vertebrate-rich Plattenkalk of Pietraröia (lower Albian, southern Apennines, Italy). *Zoological Journal of the Linnean Society*, 163, S199–S227. <https://doi.org/10.1111/j.1096-3642.2011.00718.x>
- Cerio, D. G., & Witmer, L. M. (2022). Orbital soft tissues, bones, and allometry: Implications for the size and position of crocodylian eyes. *The Anatomical Record*, 306(10), 2537–2561. <https://doi.org/10.1002/ar.25133>
- Chen, B. H., Hua, Z. H., & Li, B. H. (1985). *Chinese Alligator*. Anhui Science and Technology, Hefei.
- Chiarenza, A. A., Fabbri, M., Consorti, L., Muscioni, M., Evans, D. C., Cantalapedra, J. L., & Fanti, F. (2021). An Italian dinosaur Lagerstätte reveals the tempo and mode of hadrosauriform body size evolution. *Scientific Reports*, 11(1), 23295. <https://doi.org/10.1038/s41598-021-02490-x>
- Clark, J. M., & Norell, M. A. (1992). The early cretaceous crocodylomorph *Hylaeochampsia vectiana* from the Wealden of the Isle of Wight. *American Museum Novitates*, 3032, 1–19.
- Consorti, L., Arbulla, D., Bonini, L., Fabbri, S., Fanti, F., Franceschi, M., Frijia, G., & Pini, G. A. (2021). The Mesozoic paleoenvironmental richness of the Trieste karst. Field trip No. 4—Precongress 11-09-2021. *Geological Field Trips and Maps*, 13(1), 40. <https://doi.org/10.3301/GFT.2021.06>
- Cooper, J. S., Poole, D. F. G., & Lawson, R. (1970). The dentition of agamid lizards with special reference to tooth replacement. *Journal of Zoology*, 162, 85–98. <https://doi.org/10.1111/j.14697998.1970.tb01259.x>
- Cossette, A. P., & Brochu, C. A. (2018). A new specimen of the alligatoroid *Bottosaurus harlani* and the early history of character evolution in alligatorids. *Journal of Vertebrate Paleontology*, 38(4), 1–22. <https://doi.org/10.1080/02724634.2018.1486321>
- da Silva, O. D., da Costa, T. M., Silva-Alves, V. D., Fermiano, E. C., de Seba, M. F. R., Nogueira, O. M., Mudrek, J. R., Barbosa, A. P. D., Gusmão, A. C., Muniz, C. C., Carniello, M. A., dos Santos-Filho, M., & da Silva, D. J. (2020). Diet and food ontogeny of the lizard *Tupinambis matipu* Silva et al. 2018 (Squamata: Teiidae) in Central Brazil. *Research, Society and Development*, 9(11), e52391110073. <https://doi.org/10.33448/rsd-v9i11.10073>
- Dalla Vecchia, F. M. (2009). *Tethyshadros insularis*, a new hadrosauroid dinosaur (Ornithischia) from the upper cretaceous of Italy. *Journal of Vertebrate Paleontology*, 29, 1100–1116. <https://doi.org/10.1671/039.029.0428>
- Dalrymple, G. H. (1979). On the jaw mechanism of the snail-crushing lizards, *dracaena* Daudin 1802 (Reptilia, Lacertilia, Teiidae). *Journal of Herpetology*, 13(3), 303. <https://doi.org/10.2307/1563324>
- D'Amore, D. C. (2015). Illustrating ontogenetic change in the dentition of the Nile monitor lizard, *Varanus niloticus*: A case study in the application of geometric morphometric methods for the quantification of shape–size heterodonty. *Journal of Anatomy*, 226(5), 403–419. <https://doi.org/10.1111/joa.12293>
- de Souza, T., Leite, A., Poscai, A., & Casas, A. L. (2021). Revisiting the feeding anatomy of the semi-aquatic lizard *Dracaena guianensis* Daudin, 1801 (Reptilia, Sauria) from the Western Brazilian Amazon. *Journal of Morphological Sciences*, 38, 44–50. <https://doi.org/10.51929/jms.38.8.2021>
- Delany, M. F., & Abercrombie, C. L. (1986). American alligator food habits in northcentral Florida. *The Journal of Wildlife Management*, 50(2), 348. <https://doi.org/10.2307/3801926>
- Delfino, M., Martin, J. E., & Buffetaut, E. (2008). A new species of *Acyonodon* (Crocodylia) from the upper cretaceous (Santonian–Campanian) of Villaggio del Pescatore, Italy. *Palaeontology*, 51, 1091–1106. <https://doi.org/10.1111/j.1475-4983.2008.00800.x>
- Delfino, M., & Rook, L. (2008). African Crocodylians in the late Neogene of Europe: A revision of *Crocodylus bambolii* Ristori, 1890. *Journal of Paleontology*, 82(2), 336–343.

- Delfino, M., & Smith, T. (2012). Reappraisal of the morphology and phylogenetic relationships of the middle Eocene Alligatoroid *Diplocynodon deponiae* (Frey, Laemmert, and Riess, 1987) based on a three-dimensional specimen. *Journal of Vertebrate Paleontology*, 32, 1358–1369. <https://doi.org/10.1080/02724634.2012.699484>
- Diefenbach, O. C. (1979). Ampullarid gastropod – Staple food of *Caiman latirostris*? *Copeia*, 1979(1), 162–163.
- Drongelen, W., & Dullemeijer, P. (1982). The feeding apparatus of *Caiman crocodilus*: A functional-morphological study. *Anatomischer Anzeiger*, 151, 337–366.
- Edmund, A. G. (1960). Tooth replacement phenomena in lower vertebrates. *Royal Ontario Museum*, 52, 1–190.
- Ekdale, E. (2006). *Osteolaemus tetraspis* (On-line), Digital Morphology. http://digimorph.org/specimens/Osteolaemus_tetraspis/
- Erickson, G. M. (1996a). Incremental lines of von Ebner in dinosaurs and the assessment of tooth replacement rates using growth line counts. *Proceedings of the National Academy of Sciences of the United States of America*, 93(25), 14623–14627. <https://doi.org/10.1073/pnas.93.25.14623>
- Erickson, G. M. (1996b). Toothlessness in American alligators, alligator Mississippiensis. *Copeia*, 1996(3), 739. <https://doi.org/10.2307/1447542>
- Golcher-Benavides, J., & Wagner, C. E. (2019). Playing out Liem's paradox: Opportunistic Piscivory across Lake Tanganyikan cichlids. *The American Naturalist*, 194(2), 260–267. <https://doi.org/10.1086/704169>
- Griffin, C. T., Stocker, M. R., Colleary, C., Stefanic, C. M., Lessner, E. J., Riegler, M., Formoso, K., Koeller, K., & Nesbitt, S. J. (2021). Assessing ontogenetic maturity in extinct saurian reptiles. *Biological Reviews*, 96(2), 470–525. <https://doi.org/10.1111/brv.12666>
- Grigg, G. C., & Kirshner, D. (2015). *Biology and evolution of crocodylians*. Cornell University Press.
- Hay, O. P. (1930). *Second bibliography and catalogue of the fossil vertebrata of North America* (Vol. 2, pp. 1–1074). Carnegie Institution of Washington.
- Herrel, A., & Holanova, V. (2008). Cranial morphology and bite force in *Chamaeleolis* lizards - adaptations to molluscivory? *Zoology (Jena, Germany)*, 111(6), 467–475. <https://doi.org/10.1016/j.zool.2008.01.002>
- Holliday, C. M., Tsai, H. P., Skiljan, R. J., George, I. D., & Pathan, S. (2013). A 3D interactive model and atlas of the jaw musculature of *Alligator mississippiensis*. *PLoS One*, 8(6), e62806. <https://doi.org/10.1371/journal.pone.0062806>
- Holliday, C. M., & Witmer, L. M. (2007). Archosaur adductor chamber evolution: Integration of musculoskeletal and topological criteria in jaw muscle homology. *Journal of Morphology*, 268(6), 457–484. <https://doi.org/10.1002/jmor.10524>
- Horna, V., Zimmermann, R., Cintra, R., & Vásquez, P. (2003). Feeding ecology of the black caiman (*Melanosuchus niger*) in Manu National Park, Peru. *Lyonia*, 4(1), 65–72.
- Huang, J., Motani, R., Jiang, D., Ren, X., Tintori, A., Rieppel, O., Zhou, M., Hu, Y., & Zhang, R. (2020). Repeated evolution of durophagy during ichthyosaur radiation after mass extinction indicated by hidden dentition. *Scientific Reports*, 10(1), 7798. <https://doi.org/10.1038/s41598-020-64854-z>
- Huxley, T. H. (1875). On *Stagonolepis robertsoni*, and on the evolution of the Crocodylia. *Quarterly Journal of the Geological Society of London*, 31, 423–438. <https://doi.org/10.1144/GSL.JGS.1875.031.01-04.29>
- Iordansky, N. N. (1964). The jaw muscles of the crocodiles and some relating structures of the crocodylian skull. *Anatomischer Anzeiger*, 115, 256–280.
- Iordansky, N. N. (1973). The skull of the crocodylia. In C. Gans & T. S. Parsons (Eds.), *Biology of the Reptilia* (Vol. 4, pp. 201–284). Academic Press.
- Jouve, S., Sarigül, V., Steyer, J. S., & Sen, S. (2017). The first crocodylomorph from the Mesozoic of Turkey (Barremian of Zonguldak) and the dispersal of the eusuchians during the cretaceous. *Journal of Systematic Palaeontology*, 17(2), 111–128. <https://doi.org/10.1080/14772019.2017.1393469>
- Juuri, E., Jussila, M., Seidel, K., Holmes, S., Wu, P., Richman, J., Heikinheimo, K., Chuong, C., Arnold, K., Hochedlinger, K., Klein, O., Michon, F., & Thesleff, I. (2013). Sox2 marks epithelial competence to generate teeth in mammals and reptiles. *Development*, 140(7), 1424–1432. <https://doi.org/10.1242/dev.089599>
- Killian, M. L. (2022). Growth and mechanobiology of the tendon-bone enthesis. *Seminars in Cell & Developmental Biology*, 123, 64–73. <https://doi.org/10.1016/j.semcdb.2021.07.015>
- Kosma, R. (2004). *The dentitions of recent and fossil scincomorph lizards (Lacertilia, Squamata)—Systematics, functional morphology, paleoecology [PhD Dissertation]* (p. 187). Hannover (Germany), University of Hannover. <https://doi.org/10.15488/6387>
- Kuzmin, I. T., Boitsova, E. A., Gombolevskiy, V. A., Mazur, E. V., Morozov, S. P., Sennikov, A. G., Skutschas, P. P., & Sues, H. (2021). Braincase anatomy of extant Crocodylia, with new insights into the development and evolution of the neurocranium in crocodylomorphs. *Journal of Anatomy*, 239(5), 983–1038. <https://doi.org/10.1111/joa.13490>
- Leuzinger, L., Cavin, L., López-Arbarello, A., & Billon-Bruyat, J.-P. (2020). Peculiar tooth renewal in a Jurassic ray-finned fish (Lepisosteiformes, †*Scheenstia* sp.). *Palaeontology*, 63, 117–129. <https://doi.org/10.1111/pala.12446>
- Magnusson, W. E., da Silva, E. V., & Lima, A. P. (1987). Diets of Amazonian crocodylians. *Journal of Herpetology*, 21(2), 85. <https://doi.org/10.2307/1564468>
- Martín, J., Ortega, J., López, P., Pérez-Cembranos, A., & Pérez-Mellado, V. (2013). Fossorial life does not constrain diet selection in the amphisbaenian *Trogonophis wiegmanni*. *Journal of Zoology*, 291(3), 226–233. <https://doi.org/10.1111/jzo.12064>
- Martín, J. E. (2007). New material of the late cretaceous globidontan *Acynodon iberocitanus* (Crocodylia) from southern France. *Journal of Vertebrate Paleontology*, 27(2), 362–372. [https://doi.org/10.1671/0272-4634\(2007\)27\[362:NMOTLC\]2.0.CO;2](https://doi.org/10.1671/0272-4634(2007)27[362:NMOTLC]2.0.CO;2)
- Martín, J. E., Delfino, M., García, G., Godefroit, P., Berton, S., & Valentin, X. (2016). New specimens of *Allodaposuchus precedens* from France: Intraspecific variability and the diversity of European late cretaceous eusuchians. *Zoological Journal of the Linnean Society*, 176, 607–631. <https://doi.org/10.1111/zoj.12331>
- McCurry, M. R., Evans, A. R., Fitzgerald, E. M. G., McHenry, C. R., Bevitt, J., & Pyenson, N. D. (2019). The repeated evolution of dental apicobasal ridges in aquatic-feeding mammals and reptiles. *Biological Journal of the Linnean Society*, 127(2), 245–259. <https://doi.org/10.1093/biolinnean/blz025>
- Mehler, S. J., & Bennett, R. A. (2003). Oral, dental, and beak disorders of reptiles. *Veterinary Clinics of North America: Exotic Animal Practice*, 6(3), 477–503. [https://doi.org/10.1016/S1094-9194\(03\)00032-X](https://doi.org/10.1016/S1094-9194(03)00032-X)

- Mercolli, C., & Yanosky, A. A. (1994). The diet of adult *Tupinambis teguixin* (Saurea, Teiidae), in the eastern chaco of Argentina. *The Herpetological Journal*, 4, 15–19.
- Mesquita, D. O., Colli, G. R., Costa, G. C., França, F. G. R., Garda, A. A., & Péres, A. K. (2006). At the Water's edge: Ecology of semiaquatic teiids in Brazilian Amazon. *Journal of Herpetology*, 40(2), 221–229. <https://doi.org/10.1670/123-05A.1>
- Moran, S. (1979). A lizard, *Eumeces schneideri*, preying on the snail *Theba pisana*. *Israel Journal of Zoology*, 28, 38.
- Muscioni, M., Chiarenza, A. A., Delfino, M., Fabbri, M., Milocco, K., & Fanti, F. (2023). *Acynodon adriaticus* from Villaggio del Pescatore (Campanian of Italy): Anatomical and chronostratigraphic integration improves phylogenetic resolution in Hylaeochampsidae (Eusuchia). *Cretaceous Research*, 151, 105631. <https://doi.org/10.1016/j.cretres.2023.105631>
- Muscioni, M., Kustatscher, E., Arbull, D., & Fanti, F. (2024). A new census of the paleodiversity of the Villaggio del Pescatore lagerstätte (Campanian, Trieste). *Paleodays 2024, XXIV Edizione delle Giornate di Paleontologia, Pisa, 5–7 June 2024. Abstract book*.
- Narváez, I., Brochu, C. A., Escaso, F., Pérez-García, A., & Ortega, F. (2015). New Crocodyliforms from southwestern Europe and definition of a diverse clade of European late cretaceous basal Eusuchians. *PLoS One*, 10(11), e0140679. <https://doi.org/10.1371/journal.pone.0140679>
- Neenan, J. M., Li, C., Rieppel, O., Bernardini, F., Tuniz, C., Muscio, G., & Scheyer, T. M. (2014). Unique method of tooth replacement in durophagous placodont marine reptiles, with new data on the dentition of Chinese taxa. *Journal of Anatomy*, 224(5), 603–613. <https://doi.org/10.1111/joa.12162>
- Nesbitt, S. J. (2011). The early evolution of archosaurs: Relationships and the origin of major clades. *Bulletin of the American Museum of Natural History*, 2011(352), 1–292. <https://doi.org/10.1206/352.1>
- Neubauer, T. A., & Harzhauser, M. (2022). Onset of late cretaceous diversification in Europe's freshwater gastropod fauna links to global climatic and biotic events. *Scientific Reports*, 12(1), 2684. <https://doi.org/10.1038/s41598-022-06557-1>
- Neubauer, T. A., Hauffe, T., Silvestro, D., Schauer, J., Kadolsky, D., Wesselingh, F. P., Harzhauser, M., & Wilke, T. (2021). Current extinction rate in European freshwater gastropods greatly exceeds that of the late cretaceous mass extinction. *Communications Earth & Environment*, 2(1), 97. <https://doi.org/10.1038/s43247-021-00167-x>
- Nobre, P. H., & Carvalho, I. S. (2006). *Adamantinasuchus navae*: A new Gondwanan Crocodylomorpha (Mesoeucrocodylia) from the late cretaceous of Brazil. *Gondwana Research*, 10(4), 370–378. <https://doi.org/10.1016/j.jgr.2006.05.008>
- Ősi, A. (2008). Cranial osteology of *Iharkutosuchus makadii*, a late cretaceous basal eusuchian crocodyliform from Hungary. *Neues Jahrbuch für Geologie Und Paläontologie - Abhandlungen*, 248(3), 279–299. <https://doi.org/10.1127/0077-7749/2008/0248-0279>
- Ősi, A. (2014). The evolution of jaw mechanism and dental function in heterodont crocodyliforms. *Historical Biology*, 26(3), 279–414. <https://doi.org/10.1080/08912963.2013.777533>
- Ősi, A., & Barrett, P. M. (2011). Dental wear and oral food processing in *Caiman latirostris*: Analogue for fossil crocodylians with crushing teeth. *Neues Jahrbuch Für Geologie Und Paläontologie - Abhandlungen*, 261(2), 201–207. <https://doi.org/10.1127/0077-7749/2011/0161>
- Ősi, A., & Weishampel, D. B. (2009). Jaw mechanism and dental function in the late cretaceous basal eusuchian *Iharkutosuchus*. *Journal of Morphology*, 270(8), 903–920. <https://doi.org/10.1002/jmor.10726>
- Pauwels, O. S. G., Barr, B., Sanchez, M. L., & Burger, M. (2007). Diet records for the dwarf crocodile, *Osteolaemus tetraspis tetraspis* in Rabi oil fields and loango national park, southwestern Gabon. *Hamadryad*, 31, 258–264.
- Pitman, C. R. S. (1931). *A game Warden among his charges* (pp. 1–336). Nisbet & Co. Ltd.
- Pommery, Y., Scheyer, T. M., Neenan, J. M., Reich, T., Fernandez, V., Voeten, D. F. A. E., Losko, A. S., & Werneburg, I. (2021). Dentition and feeding in Placodontia: Tooth replacement in *Henodus chelyops*. *BMC Ecology and Evolution*, 21(1), 136. <https://doi.org/10.1186/s12862-021-01835-4>
- Poole, D. F. G. (1961). Notes on tooth replacement in the Nile crocodile *Crocodilus niloticus*. *Proceedings of the Zoological Society of London*, 136(1), 131–140. <https://doi.org/10.1111/j.1469-7998.1961.tb06083.x>
- Porter, W. R., Sedlmayr, J. C., & Witmer, L. M. (2016). Vascular patterns in the heads of crocodylians: Blood vessels and sites of thermal exchange. *Journal of Anatomy*, 229(6), 800–824. <https://doi.org/10.1111/joa.12539>
- Pregill, G. (1984). Durophagous feeding adaptations in an Amphisbaenid. *Journal of Herpetology*, 18(2), 186. <https://doi.org/10.2307/1563747>
- Puértolas-Pascual, E., Blanco, A., Brochu, C. A., & Canudo, J. I. (2016). Review of the late cretaceous-early Paleogene crocodylomorphs of Europe: Extinction patterns across the K-PG boundary. *Cretaceous Research*, 57, 565–590. <https://doi.org/10.1016/j.cretres.2015.08.002>
- Puértolas-Pascual, E., Canudo, J. I., & Moreno-Azanza, M. (2013). The eusuchian crocodylomorph *Allodaposuchus subjuniperus* sp. nov., a new species from the latest cretaceous (upper Maastriichtian) of Spain. *Historical Biology*, 26(1), 91–109. <https://doi.org/10.1080/08912963.2012.763034>
- Rice, A. N. (2004). *Diet and condition of American alligators (Alligator mississippiensis) in three central Florida lakes*. M.Sc. Thesis. (pp. 1–89). University of Florida.
- Rieppel, O. (2001). Tooth implantation and replacement in Sauropterygia. *PalZ*, 75(2), 207–217. <https://doi.org/10.1007/BF02988014>
- Rio, J. P., & Mannion, P. D. (2021). Phylogenetic analysis of a new morphological dataset elucidates the evolutionary history of Crocodylia and resolves the long-standing gharial problem. *PeerJ*, 9, e12094. <https://doi.org/10.7717/peerj.12094>
- Robinson, B. W., & Wilson, D. S. (1998). Optimal foraging, specialization, and a solution to Liem's paradox. *The American Naturalist*, 151(3), 223–235. <https://doi.org/10.1086/286113>
- Salas-Gismondi, R., Flynn, J. J., Baby, P., Tejada-Lara, J. V., Wesselingh, F. P., & Antoine, P.-O. (2015). A Miocene hyperdiverse crocodylian community reveals peculiar trophic dynamics in proto-Amazonian mega-wetlands. *Proceedings of the Royal Society B: Biological Sciences*, 282(1804), 20142490. <https://doi.org/10.1098/rspb.2014.2490>
- Sander, P. M. (1999). The microstructure of reptilian tooth enamel: Terminology, function, and phylogeny. *Münchner Geowissenschaftliche Abhandlungen*, 38, 1–102.
- Schaerlaeken, V., Holanova, V., Boistel, R., Aerts, P., Velensky, P., Rehak, I., Andrade, D. V., & Herrel, A. (2012). Built to bite: Feeding kinematics, bite forces, and head shape of a specialized

- durophagous lizard, *Dracaena guianensis* (Teiidae). *Journal of Experimental Zoology Part A: Ecological Genetics and Physiology*, 317(6), 371–381. <https://doi.org/10.1002/jez.1730>
- Scheyer, T. M., & Delfino, M. (2016). The late Miocene caimanine fauna (Crocodylia: Alligatoroidea) of the Urumaco formation, Venezuela. *Palaeontologia Electronica*, 19.3.48, 1–57. <https://doi.org/10.26879/657>
- Sellers, K. C., Nieto, M. N., Degrange, F. J., Pol, D., Clark, J. M., Middleton, K. M., & Holliday, C. M. (2022). The effects of skull flattening on suchian jaw muscle evolution. *The Anatomical Record*, 305(10), 2791–2822. <https://doi.org/10.1002/ar.24912>
- Sellers, K. C., Schmiegelow, A. B., & Holliday, C. M. (2019). The significance of enamel thickness in the teeth of *Alligator mississippiensis* and its diversity among crocodyliforms. *Journal of Zoology*, 309(3), 172–181. <https://doi.org/10.1111/jzo.12707>
- Sideleau, B., Staniewicz, A., Syah, M., & Shaney, K. J. (2022). An analysis of tomistoma (*Tomistoma schlegelii*) attacks on humans. *Marine and Freshwater Research*, 73, 1331–1338. <https://doi.org/10.1071/MF22015>
- Silveira, R. D., & Magnusson, W. E. (1999). Diets of spectacled and black caiman in the Anavilhanas archipelago, Central Amazonia, Brazil. *Journal of Herpetology*, 33(2), 181. <https://doi.org/10.2307/1565713>
- Smolensky, N. L., Fitzgerald, L., & Winemiller, K. O. (2023). Trophic ecology of African dwarf crocodiles (*Osteolaemus* spp.) in perennial and ephemeral aquatic habitats. *Journal of Herpetology*, 57(1), 60–69. <https://doi.org/10.1670/21-076>
- Sullivan, R. M., & Lucas, S. G. (2003). *Brachychampsia montana* Gilmore (Crocodylia, Alligatoroidea) from the Kirtland formation (upper Campanian), San Juan Basin, New Mexico. *Journal of Vertebrate Paleontology*, 23(4), 832–841.
- Sweetman, S., Pedreira-Segade, U., & Vidovic, S. (2014). A new bernissartiid crocodyliform from the lower cretaceous Wessex formation (Wealden group, Barremian) of the Isle of Wight, southern England. *Acta Palaeontologica Polonica*, 60(2), 257–268. <https://doi.org/10.4202/app.00038.2013>
- The Deep Scaly Project. (2006a). *Tiliqua scincoides*. Digital Morphology. http://digimorph.org/specimens/Tiliqua_scincoides/
- The Deep Scaly Project. (2006b). *Varanus exanthematicus*. Digital Morphology. http://digimorph.org/specimens/Varanus_exanthematicus/
- Thorbjarnarson, J. B. (1993). Diet of the spectacled caiman (*Caiman crocodilus*) in the central Venezuelan llanos. *Herpetologica*, 49(1), 108–117.
- Thorn, K. M., Hutchinson, M. N., Archer, M., & Lee, M. S. Y. (2019). A new scincid lizard from the Miocene of northern Australia, and the evolutionary history of social skinks (Scincidae: Egerniinae). *Journal of Vertebrate Paleontology*, 39(1), e1577873. <https://doi.org/10.1080/02724634.2019.1577873>
- Turner, A. H., & Brochu, C. A. (2010). A reevaluation of the crocodyliform *Acynodon* from the late cretaceous of Europe. *Journal of Vertebrate Paleontology*, 30(suppl 3), 179A.
- Whitlock, J. A., & Richman, J. M. (2013). Biology of tooth replacement in amniotes. *International Journal of Oral Science*, 5(2), 66–70. <https://doi.org/10.1038/ijos.2013.36>
- Whitney, M. R., & Sidor, C. A. (2019). Histological and developmental insights into the herbivorous dentition of tapinocephalid therapsids. *PLoS One*, 14(10), e0223860. <https://doi.org/10.1371/journal.pone.0223860>
- Wu, P., Wu, X., Jiang, T.-X., Elsey, R. M., Temple, B. L., Divers, S. J., Glenn, T. C., Yuan, K., Chen, M.-H., Widelitz, R. B., & Chuong, C.-M. (2013). Specialized stem cell niche enables repetitive renewal of alligator teeth. *Proceedings of the National Academy of Sciences of the United States of America*, 110(22), E2009–E2018. <https://doi.org/10.1073/pnas.1213202110>
- Wu, Y.-H., Chiappe, L. M., Bottjer, D. J., Nava, W., & Martinelli, A. G. (2021). Dental replacement in Mesozoic birds: Evidence from newly discovered Brazilian enantiornithines. *Scientific Reports*, 11(1), 19349. <https://doi.org/10.1038/s41598-021-98335-8>
- Young, M. T., Steel, L., Brusatte, S. L., Foffa, D., & Lepage, Y. (2014). Tooth serration morphologies in the genus *Machimosaurus* (Crocodylomorpha, Thalattosuchia) from the late Jurassic of Europe. *Royal Society Open Science*, 1(3), 140269. <https://doi.org/10.1098/rsos.140269>

SUPPORTING INFORMATION

Additional supporting information can be found online in the Supporting Information section at the end of this article.

How to cite this article: Muscioni, M., Chiarenza, A. A., Fernandez, D. B. H., Dreossi, D., Bacchia, F., & Fanti, F. (2024). Cranial anatomy of *Acynodon adriaticus* and extreme durophagous adaptations in Eusuchia (Reptilia: Crocodylomorpha). *The Anatomical Record*, 307(12), 3653–3684. <https://doi.org/10.1002/ar.25574>